International Journal of Biological Macromolecules 322 (2025) 146754

Contents lists available at ScienceDirect

International Journal of Biological Macromolecules

journal homepage: www.elsevier.com/locate/ijbiomac

Stimuli-responsive laccase/chitosan-*g*-PNIPAM complexes: A sustainable strategy for biodegradation of organic pollutants

Larisa-Maria Petrila [a], Maria Karayianni [a], Tudor Vasiliu [a], Răzvan Puf [a], Marcela Mihai [a,*], Stergios Pispas [a,b,*]

[a] Petru Poni Institute of Macromolecular Chemistry, Iasi, Romania
[b] Theoretical and Physical Chemistry Institute, National Hellenic Research Foundation, Athens, Greece

ARTICLE INFO

Keywords:
Trametes versicolor laccase
Chitosan
Hybrid nanostructures
Poly(N-isopropylacrylamide)
Dye degradation
Enzymatic catalysis

ABSTRACT

Hybrid nanostructures from synthetic and biological macromolecules emerged as a significant research topic as they can find applications in biomedicine, catalysis, and environmental remediation. Herein, innovative nanostructures in the form of electrostatic complexes were prepared by the interaction of laccase with a hybrid graft copolymer, CHI-*g*-PNIPAM, obtained by grafting poly(N-isopropylacrylamide) containing carboxylate end-groups onto chitosan chains. The size, charge, morphology, and stability of the obtained nanostructures were investigated through light scattering measurements and scanning transmission electron microscopy, demonstrating the effect of the ratio between the components on the properties of the obtained co-assembled nanostructures. Also, molecular dynamics simulations were performed to determine the interaction mechanism between the copolymer and the enzyme. The use of the copolymer imparted the nanostructures with improved stability in various conditions and thermo-responsive behaviour, while the incorporation of laccase into such nanostructures enhanced the catalytic activity of the enzyme. The obtained hybrid nanostructures were successfully employed as catalysts for the degradation of indigo carmine and Congo red from aqueous solutions, demonstrating their potential as novel catalysts for cutting-edge applications.

1. Introduction

The formation of polyelectrolyte complexes (PECs) represents an important topic in scientific research, as such structures can be prepared for various cutting-edge applications, including gene delivery, controlled drug release, biosensors, hybrid catalysis or environmental remediation [1,2]. The preparation of PECs is an easy method consisting of the formation of non-covalent interactions, including electrostatic and hydrophobic interactions and/or hydrogen bonds between oppositely charged components [3]. Their assembly has been exhaustively studied, the influence of various parameters being assessed, including the component ratio, charge density, ionic strength, polymer conformation, molar mass, and rate of addition of the components [4–7]. Moreover, different building blocks have been utilized, including synthetic polymers [8] or copolymers [9], polysaccharides [10,11] or proteins/enzymes [12,13].

Between the tested polyelectrolytes, polysaccharides have emerged as remarkable building blocks for the construction of PECs due to their natural origin and specific properties, including stability, biocompatibility, and biodegradability [14,15]. One of the most representative of this class is chitosan (CHI), obtained by the deacetylation of chitin, a natural polymer found in the exoskeleton of crustaceans. CHI has β-(1 → 4)-linked D-glucosamine and *N*-acetyl-D-glucosamine monomeric units, its properties being strongly dependent on the chitin source and the degree of deacetylation [16–18]. Additionally, the properties of CHI can be tuned by employing chemical modification treatments of the hydroxyl and amino functional groups, including the grafting of pendant chains to the CHI backbone [19,20]. Such tuning can impart CHI with attractive properties such as enhanced solubility [21], temperature [22] or pH responsiveness [23]. A special type of functionalities can be obtained by the grafting of poly(N-isopropylacrylamide) (PNIPAM) on the CHI backbone. PNIPAM is a renowned thermo-responsive compound, which exhibits a reversible phase transition as the temperature increases due to its characteristic structure consisting of hydrophilic amide groups and hydrophobic isopropyl groups. At temperatures below the lower critical solution temperature (LCST about 32 °C [24]), PNIPAM is in a

* Corresponding authors.
E-mail addresses: marcela.mihai@icmpp.ro (M. Mihai), pispas@eie.gr (S. Pispas).

https://doi.org/10.1016/j.ijbiomac.2025.146754
Received 28 April 2025; Received in revised form 18 July 2025; Accepted 9 August 2025
Available online 11 August 2025

hydrated soluble state due to the formation of hydrogen bonds between the amide moieties and the solvent molecules. At temperatures above its LCST, the polymer undergoes a phase transition generated by the disruption of hydrogen bonds and the enhancement of hydrophobic interactions between the isopropyl groups, which assemble in hydrophobic microdomains to reduce the interactions with the solvent [25,26]. The collapse of the polymer chains to a more compact conformation usually translates into an increased turbidity of the system. This behaviour is usually conserved upon grafting of PNIPAM to various polysaccharides and was previously confirmed by our group for the CHI-*g*-PNIPAM copolymer [22].

Similar interest is raised by the use of proteins, particularly enzymes, as building blocks for the fabrication of PECs. Enzymes are natural catalysts that exhibit a remarkable specificity for various substrates and an increased efficiency in the catalysis of multiple processes. Nevertheless, the capacity of enzymes to catalyse reactions in complex media is rather limited by their reduced stability to environmental factors such as variations in temperature, pH, or organic solvents [27,28]. The formation of PECs between polysaccharides and enzymes is of particular interest since the assembly of the two components can lead to the formation of hybrid nanostructures (HNS) with enhanced stability. The interaction of enzymes with polysaccharides can stabilise the structure and conformation of the enzymes, modulating their catalytic activity and enhancing their stability in various experimental conditions [29]. Moreover, the inclusion of enzymes in such nanostructures offers significant benefits in terms of stability. By entrapping enzymes in HNS, a better preservation of the catalytic activity can be obtained by protecting the structural integrity of the enzyme and enhancing its stability upon variation in the environmental conditions, including pH, temperature or the presence of inhibitors in the media. Moreover, the embedment of enzymes in HNS can prolong their stability upon storage, protecting the enzymes from denaturation and enhancing their operational stability. These advantages recommend the use of HNS formation as an efficient method of immobilising enzymes, as also suggested by the examples of HNS based on enzymes reported in the literature, obtained by employing lysozyme [30,31], α-amylase [32,33] or glucose-oxidase [34]. Concerning the drawbacks of this method, it is important to note that generally, the immobilisation of enzymes leads to a decrease in the catalytic activity due to steric constraints in the interaction between substrate and enzyme [35]. Additionally, the formation of soft matter systems incorporating enzymes might pose difficulties in the recovery of the biocatalyst from the reaction media.

Besides the improved stability of the embedded enzyme, such nanostructures can possess attractive properties, including biocompatibility, stimuli-responsiveness, or biodegradability generated by the use of polysaccharides, leading the path to new applications of enzyme/polysaccharide HNS, such as for drug-delivery, antimicrobial surfaces, catalysis or environmental remediation. Of increased interest is the use of such catalysts for environmental remediation purposes, especially for the decontamination of polluted water samples. The use of oxidoreductases such as laccase (LAC) and horseradish peroxidase is of particular importance in this context since the mentioned enzymes can convert various organic pollutants to less toxic derivatives, either directly or in the presence of redox mediators [36–38].

The current study investigates the formation of HNS based on the interaction between a copolymer containing CHI grafted with PNIPAM (CHI-*g*-PNIPAM) and LAC from *Trametes versicolor* fungus, providing a novel perspective on the interaction between the two components extensively investigated at different mixing ratios, by dynamic and electrophoretic light scattering (DLS, ELS) and scanning transmission electron microscopy (STEM). To the best of our knowledge, this is the first study thoroughly discussing the interaction of LAC with a thermoresponsive polysaccharide, outlining the potential beneficial effects of the PNIPAM side chains on the stabilisation of the enzyme. Further information about the mode of interaction of LAC with CHI-*g*-PNIPAM was obtained using molecular dynamics (MD) simulations, providing valuable information about the formation of the HNS and the effect of CHI-*g*-PNIPAM on the structure and stability of the enzyme. Additionally, the thermo-responsive behaviour of the HNS, imparted by the PNIPAM side chains of the CHI-*g*-PNIPAM, was studied in the 25–45 °C range, highlighting the fact that the formed HNS present thermo-responsive behaviour. The stability of the formed nanostructures to ionic strength variations, the preservation of the catalytic activity of the embedded enzyme, and the possible conformational changes in the structure of the enzyme were additionally investigated. Furthermore, the study followed the applicative potential of the so-formed HNS, discussing the potential of the formed nanostructures to catalyse the degradation of water pollutants by targeting indigo carmine (IC) and Congo red (CR) as model pollutants, a subject that has been discussed so far in the literature only briefly.

2. Materials and methods

2.1. Materials

High molar mass CHI grafted with poly(N-isopropylacrylamide) (CHI-*g*-PNIPAM, M_w = 206,800 g/mol) was synthesised in our laboratory through a "*grafting to*" approach using a radical-mediated coupling reaction between CHI and a PNIPAM obtained by RAFT-polymerisation technique [22]. LAC produced by *Trametes versicolor* fungus, 2,2′-azinobis(3-ethylbenzothiazoline-6-sulfonic acid) (ABTS) and CR were acquired from Sigma Aldrich (Germany), whereas IC was purchased from VWR Chemicals and syringaldehyde (SG) from Alfa Aesar.

2.2. HNS preparation

To obtain HNS, stock solutions of 0.5 mg/mL for LAC and 1 mg/mL for CHI-*g*-PNIPAM in acetate buffer solution (100 mM, pH = 4.5) were first prepared and left overnight to equilibrate at 4 °C. The nanostructures were prepared by mixing corresponding volumes of LAC and CHI-*g*-PNIPAM solutions at various mass ratios (MR), as presented in Table 1. After 5 min of stirring, the mixtures were diluted with acetate buffer at a final volume of 10 mL, the enzyme concentration being kept constant at 0.2 mg/mL, while the variation of CHI-*g*-PNIPAM volume led to increasing mass ratios between the two components.

2.3. DLS measurements

DLS measurements were performed using a Litesizer 500 instrument from Anton Paar (Graz, Austria) equipped with a 40 mW single-frequency laser diode operating at a 658 nm wavelength. The measurements were performed at a 90° angle and 25 °C, if not otherwise stated. The results were analysed with the Kalliope software (version 3.2.4). The measurements offered information about the scattered light intensity (directly connected to the mass of the species in solution), nanostructures sizes and distributions, and polydispersity indexes.

The stability of the formed HNS to ionic strength was analysed based on DLS measurements, performed after the addition of increasing

Table 1
Concentrations and mass ratios (MR) of LAC and CHI-*g*-PNIPAM used for the HNS preparation.

Sample code	LAC concentration (mg/mL)	LAC Volume (mL)	CHI-*g*-PNIPAM concentration (mg/mL)	CHI-*g*-PNIPAM Volume (mL)	MR CHI/LAC
HNS-2	0.20	4.00	0.40	4.00	2.00
HNS-1			0.20	2.00	1.00
HNS-0.5			0.10	1.00	0.50
HNS-0.25			0.05	0.50	0.25

amounts of 1 M NaCl solution to the initially formed HNS solutions. After the addition of exact volumes of saline solution, the samples were thoroughly mixed and left to equilibrate for 10 min before the DLS measurements.

The temperature behaviour of the CHI-*g*-PNIPAM and the HNS was analysed by performing DLS measurements as a function of temperature, in the interval 25–45 °C. The samples were heated with a 5 °C step, left to equilibrate for 10 min, and analysed by DLS.

2.4. ELS measurements

Zeta potential values were obtained by electrophoretic light scattering measurements performed using a Litesizer 500 equipment from Anton Paar (Graz, Austria), at a 175° scattering angle and room temperature.

2.5. STEM

The Verios G4 UC (Thermo Fisher Scientific, Waltham, MA, USA) scanning electron microscope in high-vacuum mode using the retractable specific detector STEM 3+ working at 20 kV was employed to evidence the morphology of the formed HNS. To prepare the samples for analysis, small aliquots of the CHI-*g*-PNIPAM solution and the HNS were deposited on 300 mesh copper grids coated with lacey carbon film and left to dry. Representative images were analysed using the ImageJ software (version 1.53 m). SEM analysis was conducted on similarly prepared samples, using the same microscope, in High Vacuum mode, using a detector for high-resolution images (Through Lens Detector, TLD) at an accelerating voltage of 15 kV and a spot size of 0.4 nA, the magnification being indicated on the micrographs.

2.6. Fluorescence spectroscopy

The structure of LAC was monitored through fluorescence spectroscopy utilizing the intrinsic fluorescence properties of the tryptophan and tyrosine amino acids of the enzyme. An excitation wavelength of λ = 280 nm was used, and the emission spectra were recorded in the 300–450 nm region with the FLS980 photoluminescence spectrometer (Edinburgh Instruments, Livingston, UK), at room temperature. From the spectra of the HNS, the corresponding contribution of the CHI-*g*-PNIPAM copolymer has been appropriately subtracted. Moreover, in an attempt to gain further information on the contribution of different tryptophan fluorophores, the spectra of the HNS were deconvoluted into a sum of Gaussian functions using the Origin software (OriginPro, Version 2019b, OriginLab Corporation, Northampton, MA, USA), following the proposed classification of tryptophan residues by Hixon and Reshetnyak [39]. Finally, the location of the individual tryptophan residues of the LAC molecule were visualized by means of the PyMOL software (PyMOL Molecular Graphics System, Version 3.0 Schrödinger, LLC), based on the crystal structure of LAC [40].

2.7. LAC activity assay

The catalytic activity of the free (initial) LAC solution and the LAC embedded in the HNS was assessed using ABTS as a model substrate. For this, the ABTS solution prepared in acetate buffer solution (pH = 4.5, 100 mM) was brought into contact with a certain volume of LAC solution or HNS dispersion. The enzymatic conversion of ABTS to $ABTS^{+}$ was followed at λ = 420 nm, using the Spekol 1300 Plus UV-VIS Spectrophotometer (Analytic Jena, Germany). One unit of activity was defined as the amount of enzyme needed to oxidize 1 μmol ABTS in 1 min. All experiments were performed in triplicate, and the average values corrected with the standard deviation were used to calculate the relative activity of the samples. The activity of the initial LAC solution was defined as 100 %, and the rest of the values were calculated in relation to that, using Eq. (1):

$$RA\ (\%) = A_{HNS}/A_{LAC}\cdot 100 \quad (1)$$

where: RA – relative activity, A_{HNS} (U) – observed activity of the HNS under assay conditions and A_{LAC} (U) – observed activity of the LAC solution under assay conditions. All the experiments were done in triplicate, and the mean values corrected with the standard deviation are presented.

The effect of pH on the catalytic activity of the free LAC and the HNS was assessed using the same method described above, in the pH range of 3.5–6.5. All experiments were performed in triplicate, and the average values, corrected for standard deviation, are presented.

The temperature influence on the activity of the free LAC and the HNS was assessed after incubating the samples for 15 min at temperatures varying between 25 °C and 60 °C, followed by cooling at room temperature and assessment of the residual catalytic activity using the same method as described above.

The kinetic parameters of LAC before and after the formation of HNS were assessed under optimal reaction conditions, using ABTS as substrate, in a concentration range of 0.1 to 1 mM. The kinetic parameters, K_m and V_{max} were calculated from the Lineweaver-Burk plot, using a linear regression fitting model. The turnover number (k_{cat}) was calculated employing Eq. (2):

$$k_{cat} = V_{max}/[E] \quad (2)$$

where: k_{cat} – the turnover number, V_{max} – maximum reaction velocity, [E] – enzyme concentration in the assay (μM). All the experiments were done in triplicate, and the mean values corrected with the standard deviation are presented.

The storage stability of LAC solution and the HNS was evaluated by assessing the catalytic activity of each sample after storage for 50 days at 4 °C. The catalytic activity was determined using the method described above, and the residual activity of each sample was calculated using Eq. (3):

$$ReA\ (\%) = A_{50}/A_1\cdot 100 \quad (3)$$

where: ReA – residual activity, A_{50} (U) – observed activity of the HNS or LAC solution after 50 days of storage and A_1 (U) – observed activity of the HNS or LAC solution on the first day. All the experiments were done in triplicate, and the mean values corrected with the standard deviation are presented.

2.8. Dye degradation in the presence of LAC and HNS

To test the potential use of the HNS on water cleaning applications, the enzymatic degradation of two dyes, IC and CR, was studied as compared with that of free LAC. For this, stock solutions of IC and CR (50 mg/L) were prepared in MilliQ water and brought into contact with a volume of initial LAC solution or selected HNS, in the presence of SG as a redox mediator. The samples were kept in the dark for various time intervals, and then the degradation of the dye was assessed by registering the absorbance at λ = 610 nm (for IC) and at λ = 498 nm (for CR), using the Spekol 1300 Plus UV-VIS Spectrophotometer (Analytic Jena, Germany). The degradation efficiency (DE) was calculated using Eq. (4):

$$DE\ (\%) = (A_i – A_t)/A_i\cdot 100\ (\%) \quad (4)$$

where: A_i and A_t are the initial dye absorbance and the absorbance of the dye after t minutes, respectively. Additionally, the pseudo-first order kinetic model (Eq. (3)) was employed to describe the dye degradation process, and the degradation rate constant was calculated from the slope of the $\ln(C_t/C_0) = f(t)$ plot, based on Eq. (5):

$$\ln(C_t/C_0) = -k\cdot t \quad (5)$$

where: C_0 (mg/L) and C_t (mg/L) are the initial dye concentration and the concentration of the dye at time t (min), and k is the rate constant.

2.9. Molecular dynamics simulations

To better understand the interactions that govern the formation of the HNS between LAC and CHI-*g*-PNIPAM, molecular dynamics simulations were performed to assess the LAC behaviour in the presence of CHI-*g*-PNIPAM. Considering the large size of the CHI-*g*-PNIPAM copolymer, it is impractical to perform simulations of the full-length molecule. Therefore, to focus on the key interactions between LAC and the copolymer, a copolymer was built, consisting of 30 CHI monomers and 25 PNIPAM monomers. This approach allowed the capture of the essential intermolecular interactions while reducing the computational demands of the simulations. The simulations were performed employing the AMBER GAFF2 forcefield for the polymers, and the FF19SB forcefield for the enzyme and the TIP3P water model. To obtain the structure of the LAC enzyme 1KYA pdb, from RCSB was used [41]. The CHI-*g*-PNIPAM was built and parametrised using AmberTools [42]. The simulations were performed using the GROMACS 2024.2 software [43] with temperature set at 300 K, using V-rescale temperature coupling with a time constant of 0.5 ps. The pressure was controlled by the Parrinello–Rahman barostat and isotropic pressure coupling, with a constant time of 2.0 ps and compressibility of 4.5 × 10–5. The simulation was performed for 200 ns with an integration timestep of 2 fs.

3. Results and discussions

3.1. Formation of the HNS

The capacity of the LAC/CHI-*g*-PNIPAM pair to form electrostatic interactions, as complementary charged molecules, was studied by means of ELS measurements for the initial LAC and CHI-*g*-PNIPAM solutions prepared in acetate buffer, as depicted in Fig. 1.

Enzymes possess polyelectrolyte, or in better terms, polyampholyte characteristics as their amino acid sequences are comprised of ionizable residues. The net charge of an enzyme depends on its isoelectric point (IEP), with enzymes being positively charged below the IEP and negatively charged above it. Nonetheless, enzymes contain both positively and negatively charged amino acids, the overall charge of an enzyme depending strongly on the pH of the environment. The performed zeta potential measurements (Fig. 1) highlight that LAC has an IEP at pH ~ 3, correlated well with values reported in the literature [44,45]. At lower pH values, the acidic residues and the amino groups are protonated, leading to a net positive charge of the enzyme. At higher pH values, the deprotonation of the carboxyl groups led to the net negative charge of the enzyme, which increases with the pH increase. Nevertheless, it can be observed that the zeta potential values are rather low (up to −8 mV), suggesting the partial compensation of the charged surface functional groups of the enzyme due to the coexistence of negatively and positively charged residues, a property often observed in the case of proteins [46,47]. In the case of the grafted polysaccharide, CHI-*g*-PNIPAM, the positive character of the molecule can be observed on a large pH interval (Fig. 1), with IEP at pH ~ 7, generated especially by the ionization of the CHI backbone functional amino groups. As previously reported, the grafting of PNIPAM chains on the CHI backbone does not strongly influence the ionization degree of the copolymer, as there are approximately 14 PNIPAM chains grafted on each CHI chain and approximately 846 deacetylated monomeric units bearing chargeable amino groups [22]. Moreover, LAC can potentially interact by either electrostatic, hydrogen bonding or hydrophobic interactions with the functional groups of CHI and PNIPAM side chains as well as with the residual acetylated monomeric units of the CHI chain. Based on the variation of the zeta potential as a function of pH, it can be assumed that the positively charged CHI-*g*-PNIPAM should be able to interact with LAC, leading to the formation of electrostatic complexes in the pH range 3–7. Nevertheless, to protect the enzyme from eventual denaturation and loss of enzymatic activity, the studies were performed at pH = 4.5.

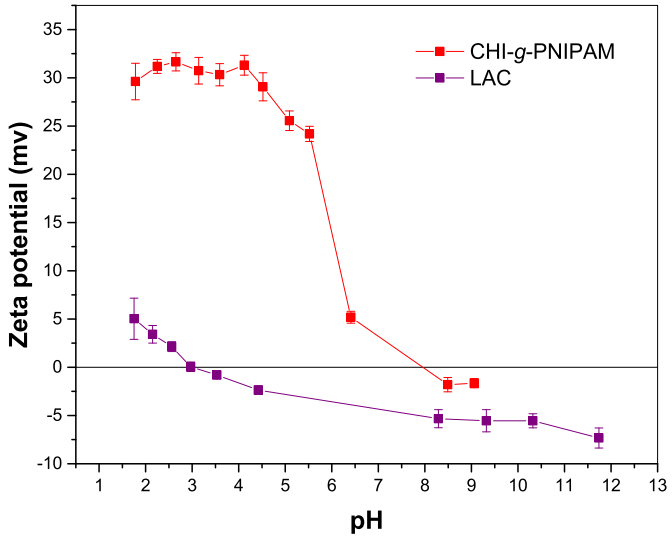

Fig. 1. Zeta potential as a function of pH for LAC and CHI-*g*-PNIPAM solutions.

The successful formation of HNS by the interaction of LAC and CHI-*g*-PNIPAM can be tracked via DLS measurements, by analysing the variation of the scattered intensity of the samples, as the increase in scattered intensity can be correlated with an increase in the mass of the nanostructures detected during measurements. Fig. 2a presents the scattered intensity of the HNS solutions prepared at pH = 4.5.

The formation of the HNS at the selected pH is directly confirmed by the augmented values in the scattered intensity, which increases with the increase in the amount of CHI-*g*-PNIPAM utilized, suggesting the formation of entities of greater mass. As concerns the size of the formed HNS, the intensity-weighted size distribution profiles (Fig. 2b) reveal the co-existence of two populations for both initial LAC and CHI-*g*-PNIPAM solutions and the formed HNS. The corresponding polydispersity index values are in the range of 0.2 to 0.3, indicating a rather large size polydispersity in the samples, which is directly correlated to the presence of more than one scattering population in solution. In the case of the initial LAC solution (Fig. 2b, purple), the nanostructures (6–7 nm) can be considered individual LAC molecules, as also reported in other studies [44,48], whereas the larger entities (about 200–300 nm) might be generated by the formation of enzyme aggregates [49] or by the presence of impurities or additives in the enzyme preparation. For the CHI-*g*-PNIPAM solutions (Fig. 2b, red), a two-peaks distribution can also be observed. The peaks could most probably be correlated with various possible grafted copolymer chain conformations which can be adopted, mainly given by the backbone semi-rigid conformation, interchains and/or intrachain electrostatic binding/bridging between carboxylate end group of the PNIPAM side chains and the amino groups of the chitosan backbone, electrostatic repulsions between the protonated amino groups, hydrophobic interactions stemming from the PNIPAM side chains. Similarly, the HNS prepared at pH = 4.5 present two populations, which can be attributed to the interaction between individual constituents of the LAC and CHI-*g*-PNIPAM solutions, respectively, or the formation of complexes comprising different numbers of individual components. As expected, the increase in the amount of CHI-*g*-PNIPAM is accompanied by an increase in the size of both populations of the formed nanostructures.

Nevertheless, the formation of HNS does not lead to massive entities as observed from the size distributions, where the populations of the HNS are somewhat smaller in size compared to the corresponding populations of CHI-*g*-PNIPAM, suggesting some degree of shrinking as a result of the reduction of electrostatic repulsions due to charge neutralisation upon complexation.

The MD simulation performed for the system containing LAC, CHI, and PNIPAM corroborates these findings. The simulation of LAC in the

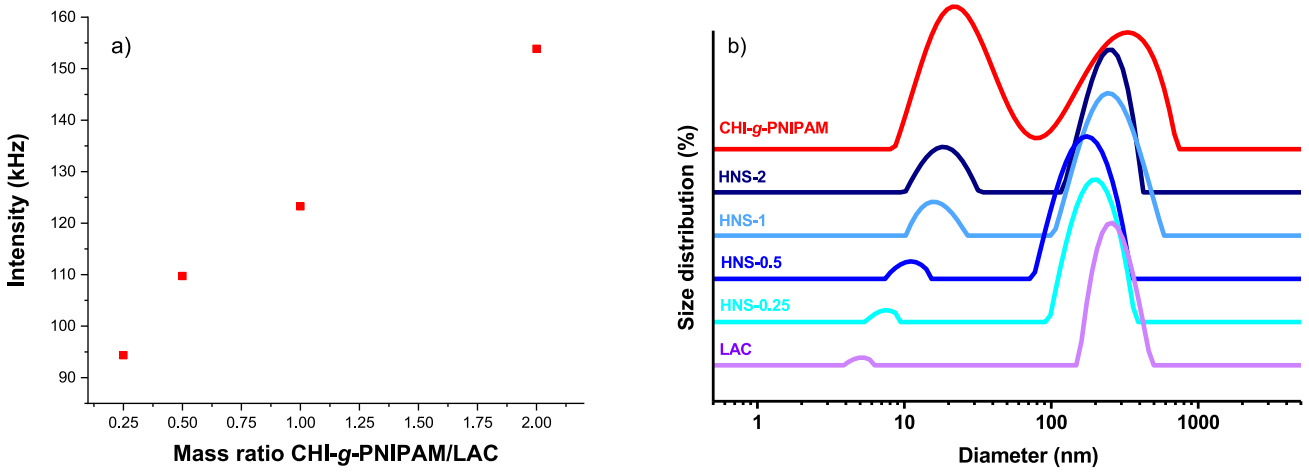

Fig. 2. Scattered intensity (a) and size distributions (b) for the HNS.

presence of the copolymer, started with the random distribution of 4 CHI-*g*-PNIPAM molecules around the enzyme, is presented in Fig. 3a. By the end of the simulation presented in Fig. 3b, it can be observed that the formation of the HNS occurs based on the interaction between the copolymer and the enzyme.

MD simulations revealed two key findings: (1) both CHI and PNIPAM interact with the enzyme, and (2) these interactions occur at the enzyme's surface, as evidenced in Fig. 4.

As with any protein, there is a strong correlation between LAC structure and its enzymatic activity. To test the influence of the interaction between CHI-*g*-PNIPAM and LAC on the structure of the enzyme, a Root Mean Square Deviation analysis (RMSD) was performed, as presented in Fig. 5. It can be seen that the RMSD increases slowly at the beginning of the simulation, to a value of ~2.5 Å, but this is to be expected as the enzyme adapts to the solvent environment. Once this adaptation finishes, the RMSD remains constant. It can be concluded that the surface interactions between the LAC and the copolymer do not induce protein denaturation.

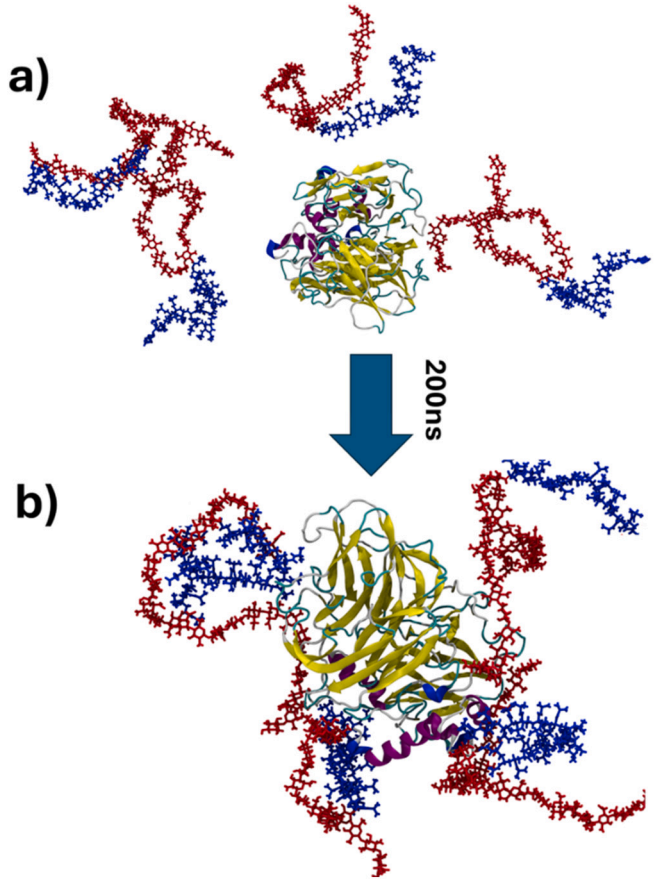

Fig. 3. Snapshot depicting the starting conformation of the enzyme-copolymer system (a) and snapshot depicting the LAC/CHI-*g*-PNIPAM complex obtained after 200 ns of interaction (b). The enzyme is depicted in new-cartoon representation, the CHI is coloured in red, and the PNIPAM is coloured in blue.

Additional information about the HNS prepared was obtained based on zeta potential measurements, which reflect the effective charge of the formed nanostructures and offers important information about the possible electrostatic interactions between LAC and CHI-*g*-PNIPAM. Notably, as shown in Fig. 6, HNS exhibit positive zeta potential values, varying approximately between +16 and + 26 mV. The zeta potential of the HNS slightly increases with the increase in the CHI-*g*-PNIPAM content, demonstrating that the positive charge of the CHI backbone, which is in excess due to the high charge density of the polysaccharide, dictates the overall surface charge of the formed nanostructures. This can also be seen in Figs. 3 and 4 of the simulation, where it is clear that the CHI is electrostatically linked at the surface of the enzyme, leading to a net positive charge on its surface. Also, the effective charge of the HNS is somewhat smaller than that of the graft copolymer, demonstrating partial charge neutralisation due to the CHI-*g*-PNIPAM complexation with the oppositely charged surface patches of the LAC molecules and confirming the absorption of the polymer at the surface of the enzyme. A similar effect was observed by Panganiban et al., who studied the interaction of a random copolymer and horseradish peroxidase, emphasising the role of the surface interaction with the polymer in the preservation of the structural integrity of the enzyme as well as in the maintenance of the catalytic activity after incubation in organic solvents [50].

3.2. Morphology of the HNS

The morphology of the HNS-0.5 and HNS-2 was evidenced by STEM, Fig. 7 revealing the formation of almost spherical shaped HNS. Also, the HNS present a dense internal structure, a fact that serves as further proof of the successful formation of the nanostructures by LAC embedment. The STEM micrographs also highlight the presence of nanostructures of different sizes, with larger nanostructures being more easily detected in the STEM micrographs due to the better contrast, and consistent with the size distribution profiles (Fig. 2b) and the polydispersity of the samples observed by DLS. As concerns the nanostructures size, the STEM micrographs reveal that the detected nanostructures are generally smaller as compared to the populations observed in the DLS size

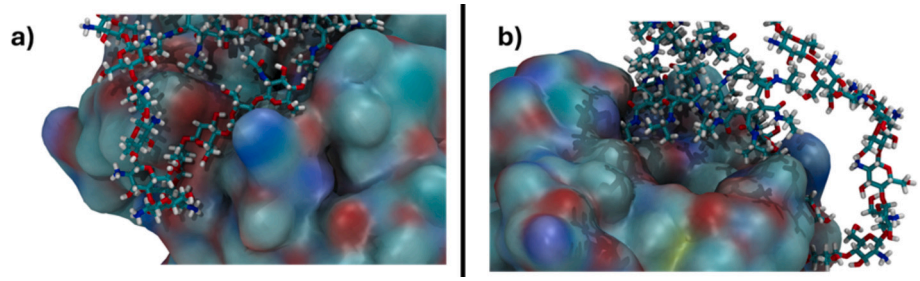

Fig. 4. Detail depicting CHI interacting with LAC (a) and detail depicting PNIPAM interacting with LAC (b). The enzyme is depicted as a solid surface, and the copolymer is depicted in liquorice style. The N atoms are coloured in blue, the O atoms are coloured in red, the C atoms are coloured in teal, and the H atoms are coloured in white for the copolymer. The enzyme surface follows the same colouring scheme.

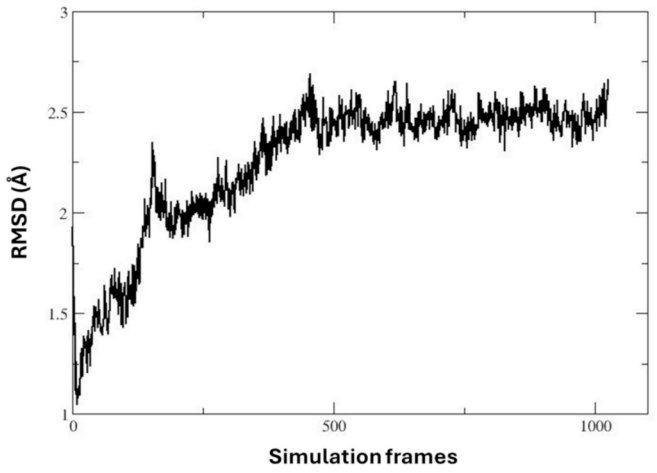

Fig. 5. RMSD evolution of the enzyme.

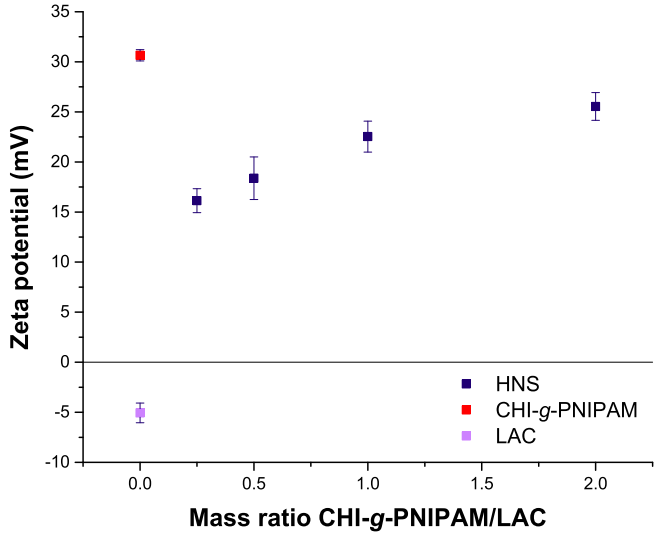

Fig. 6. Zeta potential values of the HNS prepared at pH = 4.5, along with the corresponding values for the pure LAC and CHI-*g*-PNIPAM components for comparison.

distributions (Fig. 2b) and vary between 120 and 250 nm for the larger HNS. This difference in sizes is attributed to the shrinkage of the nanostructures during solvent evaporation, a common phenomenon in such systems. The analysis of lower magnification STEM images of the same samples with the aid of ImageJ software provides additional information regarding the size and shape distribution of the detected nanostructures, as shown in Fig. S1, while the SEM micrographs presented in Fig. S2 emphasise the organisation of the nanostructures on clusters upon drying. Both HNS samples exhibit increased size polydispersity, with different populations being discerned. Specifically, for the HNS-2, a small population with an average diameter of about 20 nm and a larger one of about 80 nm can be separated, while in the case of the HNS-0.5 sample, three populations with average diameters of about 10, 30, and 90 nm are detected. Nevertheless, in both cases, the spherical shape of the nanostructures is rather uniform, corresponding to an average circularity of about 0.9.

3.3. Thermo-responsive behaviour of the HNS

As previously confirmed by our team, the CHI-*g*-PNIPAM copolymer possesses thermo-responsiveness due to the grafting of the PNIPAM side chains on the CHI backbone [22]. Since the formation of electrostatic complexes is not expected to affect the copolymer properties, it is assumed that the HNS formed based on CHI-*g*-PNIPAM would also possess a thermo-responsive behaviour, a property that can impart additional applications to the formed HNS. This behaviour can easily be evidenced by analysing the scattered intensity and sizes of the HNS upon heating, as recorded from DLS measurements.

As presented in Fig. 8a, the increase in temperature above 30–32 °C induces an important increase in the scattered intensity of both CHI-*g*-PNIPAM and the HNS, confirming the transition of the PNIPAM side chains on the copolymer from the hydrated to dehydrated state. This transition subsequently leads to the formation of more dense/compact structures of the graft copolymer molecules and of the HNS comprised of LAC and CHI-*g*-PNIPAM, respectively. This observation confirms that the HNS present thermoresponsive behaviour. The further increase of temperature above 32.5 °C does not significantly affect the scattered intensity of the HNS up to 45 °C, while upon cooling back to room temperature, the intensity abruptly drops to the initial values (values marked on the graph as 25 AH – after heating), confirming the fully reversible thermal transition of the investigated systems.

The strengthening of hydrophobic interactions generated by the increase in temperature, mostly stemming from the thermoresponsive character of the PNIPAM side chains, induces the collapse of the copolymer chains in the already formed nanostructures, with the formation of secondary aggregates that are slightly larger. This phenomenon occurs in both CHI-*g*-PNIPAM and HNS cases and is evidenced in the size distributions of the HNS (Fig. 8b and c), where the transition of the system from two populations to only one is observed. The size of the temperature-induced secondary aggregates of the HNS is rather stable upon further heating, suggesting the transition of the system from loose structures to more dense aggregates. This transition to more compact/dense structures upon heating could be proven beneficial for the protection of the enzyme against thermal unfolding/denaturation. Notably, upon cooling, the initial sizes were partially restored, displaying the reversible aggregation and solubilization behaviour of the HNS. The reversibility of the observed transition is a good indication of the

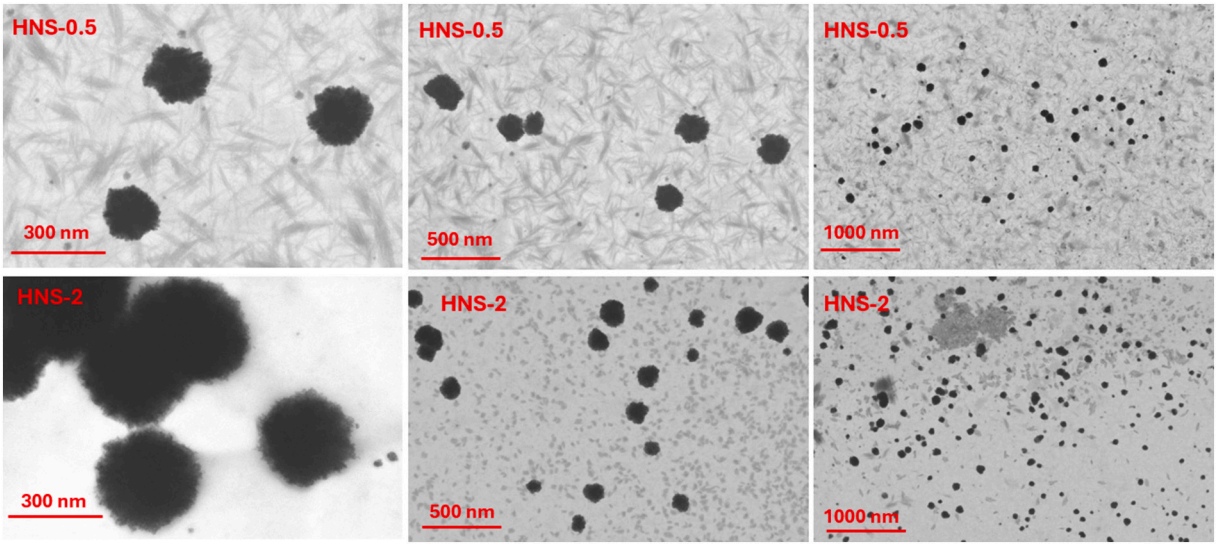

Fig. 7. STEM micrographs of the HNS-2 and HNS-0.5.

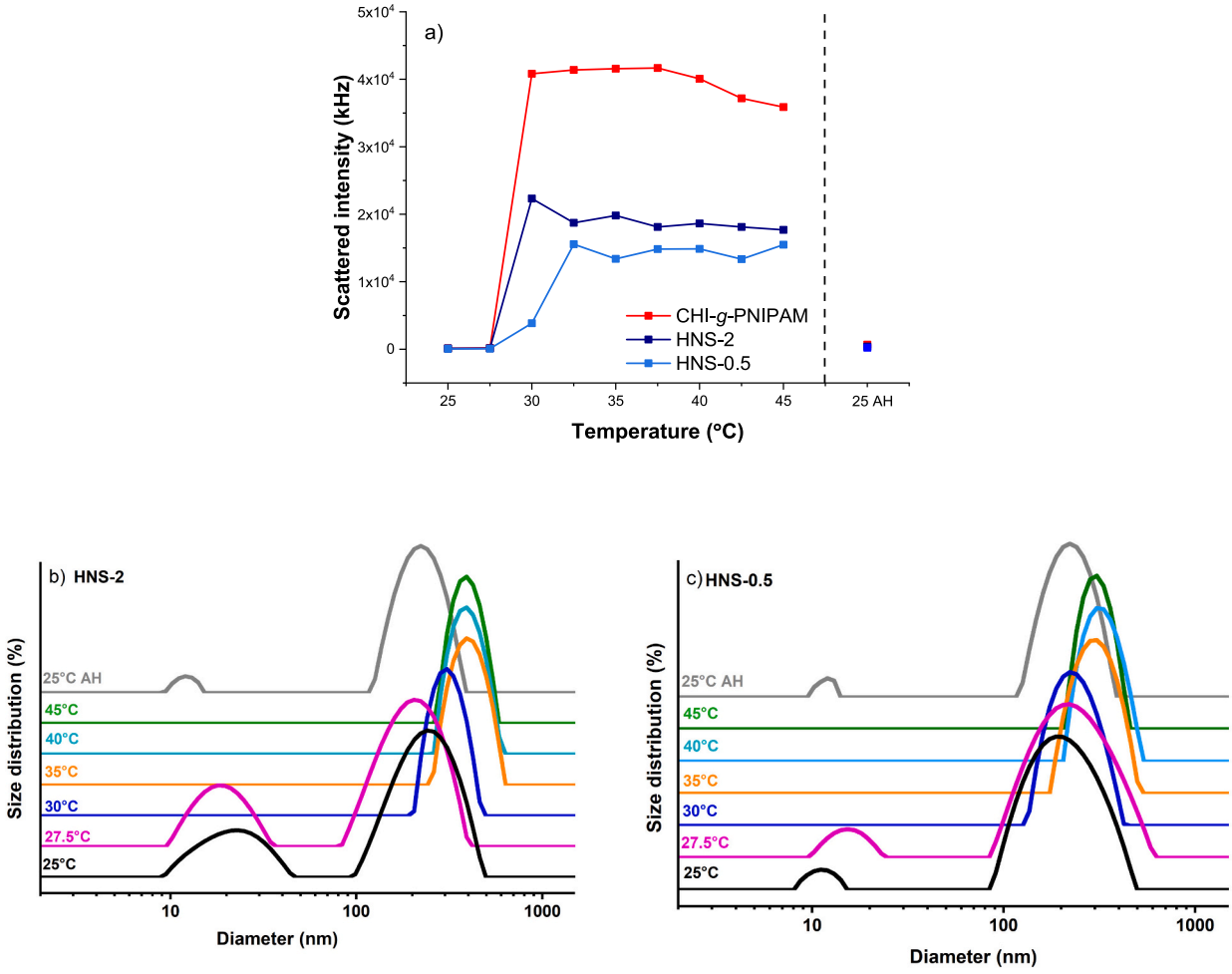

Fig. 8. Influence of temperature on the scattered intensity (a) and size distributions (b, c) of the HNS-2 and HNS-0.5.

preservation of the grafted copolymer properties after the complexation with LAC, suggesting that this property can potentially be used for the design of novel applications of the prepared HNS, relevant to their thermal stability.

3.4. Stability of the HNS against ionic strength

The stability of the HNS in various environmental conditions, including variation in ionic strength, temperature or solvent, is an important aspect to be considered for the potential applications of

nanostructures obtained based on electrostatic interactions. An important parameter to take into consideration is the ionic strength of the environment as its increase generates a shielding effect on the charged entities, thus reducing the potential interactions between oppositely charged compounds, which can in turn lead to the disruption of the formed interactions and the disassembly of the constructed HNS [51]. Additionally, the increase in ionic strength can potentially affect the already formed electrostatic complexes, which might adopt a looser conformation or can dissociate due to the electrostatic repulsions and the electrostatic screening of the counterions, which weakens the attraction between the components in the complexes [3,52]. In this context, the stability of the formed HNS to the increase of ionic strength was studied by titrating the systems with aliquots of saline solution, followed by DLS measurements.

As presented in Fig. 9a, up to an added amount of salt corresponding to 0.3 M, both CHI-*g*-PNIPAM and the HNS exhibit no significant changes in the scattered intensity, which is a good indication of their stability. Upon further increasing the ionic strength in the system, an important increase in the scattered intensity can be observed, which is correlated with an increase in the turbidity of the system, stemming from the characteristic hydrophobic behaviour of the PNIPAM side chains on the copolymer. The same behaviour is observed in the case of the HNS, confirming that the properties of the copolymer are conserved upon the complexation of LAC.

This behaviour is confirmed by the size distribution profiles of the HNS (Fig. 9b and c), which show that for ionic strength values greater than 0.4 M, a transition from two peaks to only one peak at high size values occurs. This behaviour can be attributed to the collapse of the LAC/CHI-*g*-PNIPAM aggregates with increasing ionic strength, which is a result of the increase in hydrophobic interactions between PNIPAM side chains of the copolymer. A similar behaviour was observed in the case of the copolymer, as seen in the size distribution profiles presented in Fig. S3. Apparently, the occurring strengthening of the hydrophobic interactions in the system imposed by the increase of ionic strength hinders the dissociation of the formed HNS and thus contributes to their stability.

3.5. Storage stability of the HNS

Regarding the stability of the prepared HNS, the solutions of the samples seem stable, without any macroscopic sign of phase separation or precipitation for several days, as also evidenced by the DLS and ELS results of measurements obtained after 50 days of storage at 4 °C (Fig. S4). As seen in Fig. S4a and c, there is a small decrease in the scattered intensity accompanied by a similar reduction in the relative contribution of the larger peak to the overall size distribution, which could indicate a small degree of precipitation of the larger entities in solution that are inevitably more prone to colloidal instability. Nevertheless, no significant changes in the respective sizes of the different populations are observed, apart from a slight increase of the smaller population in the case of the HNS-0.5 sample, which can be correlated to some extent of secondary aggregation. Moreover, the positive effective charge of the HNS is preserved, with only small alterations in the corresponding values of the zeta potential being detected (Fig. S4b). Likewise, the morphology of the formed nanostructures is similar to that of the freshly prepared samples, as evidenced by the obtained STEM micrographs presented in Fig. S4d and e. Altogether, the prolonged stability of the formed HNS can be attributed to the combination of

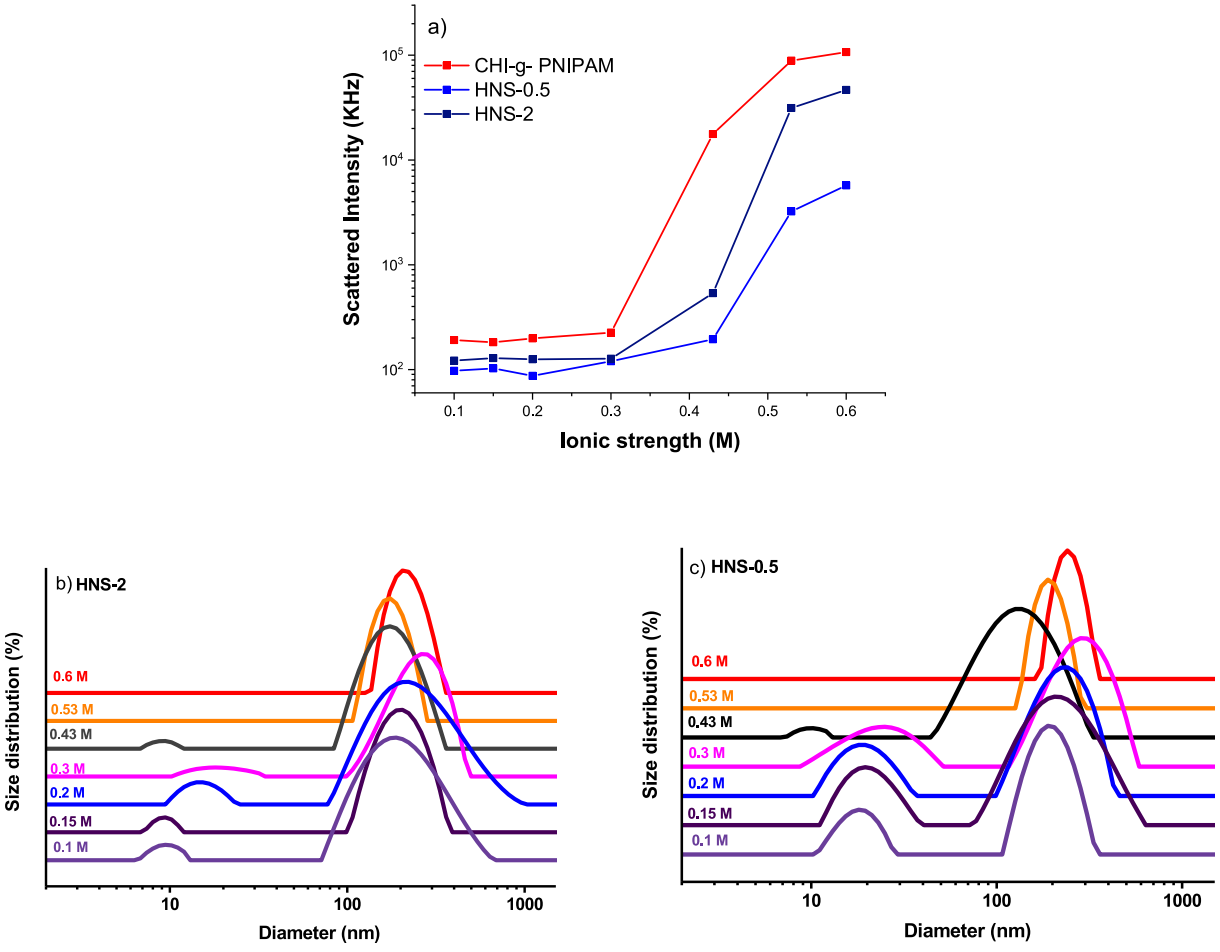

Fig. 9. Influence of the ionic strength on the scattered intensity (a) and size distributions (b, c) of the HNS-2 and HNS-0.5.

electrostatic and hydrophobic (further enhanced in this case by the presence of the PNIPAM copolymer side chains) interactions at play between the enzyme and the graft copolymer.

3.6. Catalytic activity and conformational changes of LAC embedded in the HSN

An important aspect that concerns the stabilisation of enzymes in electrostatic complexes is the potential preservation of their catalytic activity. Thus, the catalytic activity of the LAC embedded in complexes with CHI-*g*-PNIPAM was studied using a model reaction consisting of the enzymatic oxidation of ABTS. Fig. 10 presents the catalytic activity of the initial LAC solution and that of the HNS prepared based on LAC and CHI-*g*-PNIPAM.

As observed in Fig. 10, the enzymatic activity is slightly enhanced upon the complexation of LAC with CHI-*g*-PNIPAM and is more pronounced as the amount of CHI-*g*-PNIPAM in the HNS increases. This result suggests that the presence of the grafted polysaccharide has a positive effect on the enzyme activity. As already known, the complexation of enzymes with oppositely charged compounds can enhance their catalytic activity by enhancing the accessibility of the substrate towards the active site or by stabilising the active site of the enzyme [29]. The accessibility of the substrate can additionally be enhanced in the presence of enzyme-based complexes by creating an optimal environment for the catalytic reaction, producing effects such as the modification of the pH towards an optimal value, the reduction of electrostatic repulsions between the enzyme and the substrate or the enhancement of secondary interactions that facilitate the binding of the substrate to the enzymatic catalytic center. While usually enzyme binding to solid supports or enzyme conjugation to macromolecules leads to a decrease in the expressed catalytic activity [53–55], the formation of complexes can generate enhanced catalytic activity due to the stabilisation of the enzyme structure in a more accessible conformation. A similar effect was observed by Waltmann and collaborators who studied the interaction between PETase, a PET-degrading enzyme, and a random copolymer containing oligo-ethyl glycol methacrylate, ethyl hexyl methacrylate and sulfo-propyl methacrylate units [29]. Their study confirmed that the interaction between the enzyme and the random copolymer leads to increased stability of the catalytic center demonstrated by the increase in the catalytic activity observed under various experimental conditions. In another study, Wan et al. proposed the incorporation of uricase in polyion complex vesicles formed by poly(ethyleneimine) and PSS_{96}-*b*-PEO_{113} block copolymer, observing a 1.5-fold increase in the catalytic activity compared with the free enzyme, accompanied by a slight enhancement in the turnover number and a notable increase in temperature stability [56].

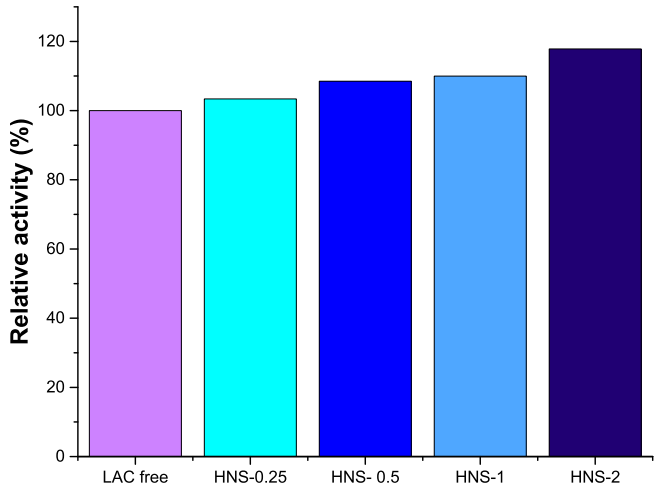

Fig. 10. Relative enzymatic activity of the LAC solution and the HNS.

The Michaelis-Menten kinetic model was employed to assess the substrate-binding affinity and the catalytic efficiency of the LAC/CHI-*g*-PNIPAM HNS. The Michaelis-Menten constant (K_m) and the maximum reaction rate (V_{max}) were determined for the Lineweaver-Burk plot (Fig. S5), and the turnover number was calculated based on the obtained kinetic parameters (Table 2). We recall that the values of the kinetic parameters depend on the experimental conditions, the enzyme structure and the substrate used.

As previously reported, V_{max} is the maximum reaction velocity obtained when the enzyme is fully saturated with the substrate, and K_m is the substrate concentration corresponding to half of the maximum reaction velocity [57]. K_m offers important information about the binding affinity between the enzyme and substrate, while k_{cat} effectively indicates the catalytic efficiency of the free or complexed enzyme. As observed from the values in Table 2, the Michaelis-Menten constant value is lower for the HNS compared with the free LAC. While generally, the immobilisation of enzymes leads to increasing values of K_m due to steric constraints in the substrate-enzyme interaction, the lower values of K_m possibly indicate a higher binding affinity between the substrate and the enzyme. Moreover, an increase in the V_{max} and k_{cat} for the HNS can be observed, suggesting an increased catalytic efficiency of the HNS, as also indicated by the catalytic activity assays in Fig. 10. It can be noticed that the amount of CHI-*g*-PNIPAM used in the complex formation plays an important role in the preservation of the catalytic activity of LAC. While higher amounts of CHI-*g*-PNIPAM determine a more important increase in the observed catalytic efficiency, the use of lower amounts of CHI-*g*-PNIPAM mostly preserves the catalytic activity of LAC, as demonstrated by the constant values of k_{cat} and V_{max} for free LAC and HNS-0.5. A similar trend in the variation of the kinetic parameters was reported by Veselova et al., who studied the formation of electrostatic complexes between horseradish peroxidase and CHI, assuming that the observed variations can be correlated with the activation of the enzyme in the presence of the polysaccharide [58].

The variation of pH can strongly influence the enzymatic activity as it can affect the ionization state of both the enzyme and the substrate and potentially affect the interaction between them. The effect of the pH on the catalytic activity of LAC and the HNS was assessed in the 3.5–6.5 interval, using the oxidation of ABTS as a model catalytic reaction.

As evidenced in Fig. 11, the pH has a strong effect on both the free LAC and the HNS. The enzymatic activity exhibits a clear dependence on pH, with a consistent trend observed for both systems. The highest enzymatic activity was registered at pH = 3.5, highlighting the importance of the acidic conditions in the preservation of the catalytic performance. Moreover, the highest enzyme activity was registered at pH = 3.5 for both free LAC and LAC embedded in the HNS, demonstrating that the complexation with CHI-*g*-PNIPAM does not strongly alter the properties of the enzyme. Further increase in the pH leads to a progressive decrease in enzymatic activity, probably due to the decrease in binding activity between the enzyme and the substrate. Additionally, the increase in pH can determine structural changes in both free enzyme and the HNS, leading to a significant loss in the enzymatic activity. Nevertheless, it can be observed that the catalytic activity of the HNS is higher at all the pH values as compared to the free enzyme, suggesting that the complexation with CHI-*g*-PNIPAM induced a positive effect on the enzyme, protecting it from the variation in the environmental conditions.

Table 2
Kinetic parameters for free LAC and HNS, assessed in optimum reaction conditions.

System	K_m (μM)	V_{max} (μM/sec)	k_{cat} (sec^{-1})
Free LAC	41.83	0.109	0.038
HNS-2	35.86	0.123	0.043
HNS-0.5	17.18	0.109	0.038

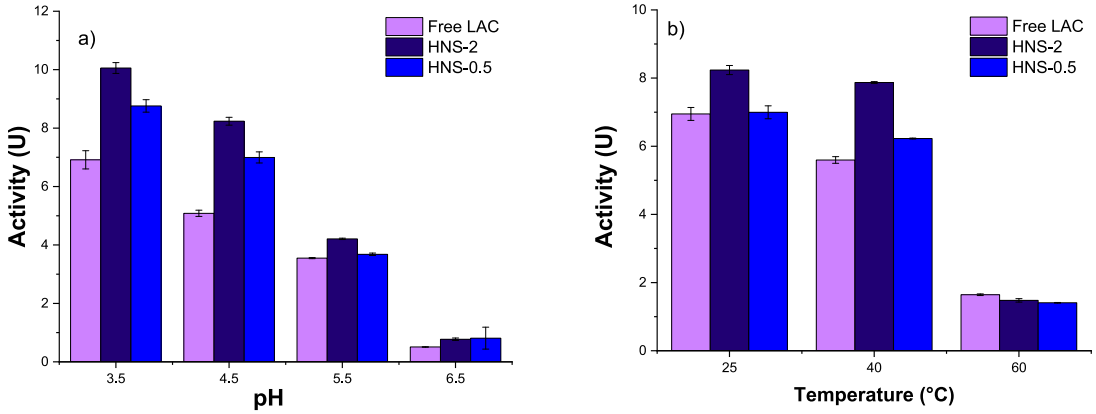

Fig. 11. Effect of the pH (a) and temperature incubation (b) on the catalytic activity of LAC solution and the HNS.

Temperature is a parameter that can potentially affect the enzymatic activity of both free and immobilised enzymes. The increase in temperature can lead to the disruption of secondary interactions that stabilise the structure of the enzyme or promote the unfolding of the enzyme molecule. The thermal stability of the LAC in solution and the HNS was evaluated by assessing the enzymatic activity after incubating the samples at various temperatures for 15 min. The residual enzymatic activity after incubation is presented in Fig. 11b. The incubation of LAC and the HNS at higher temperatures (i.e., 60 °C) leads to an important decrease in the enzymatic activity. Most likely, the reduction in enzymatic activity is caused by the disruption of the tertiary structure of the enzyme, with the parallel alteration of the active site under the effect of temperature. This effect is expected considering that the enzyme was exposed to higher temperatures, as well as the fact that the increase in temperature determines a phase transition of the PNIPAM side chains, which can generate rearrangements of the copolymer chains around the enzyme, potentially hindering the accessibility of the catalytic center. However, the catalytic activity of the HNS incubated at temperatures ≤40 °C is higher as compared to the catalytic activity of the LAC solution incubated in similar conditions, highlighting the potential beneficial effect of CHI-*g*-PNIPAM complexation and the thermal transition of the PNIPAM side chains on the characteristics of the enzyme, as also observed for the pH variation. A similar effect was also reported by Jia et al., who immobilised LAC in polymeric nanogels, observing a better stabilisation of the enzyme embedded in the nanogel compared with the free enzyme at both pH and temperature variations [59].

Another important aspect to consider concerning biocatalysts is their long-term storage stability. Generally, upon storage, enzymes lose their catalytic activity due to a combination of factors, including the degradation or unfolding of the amino acid sequence of the enzyme, with the distortion of the catalytic center, negative effects generated by pH, temperature or light exposure, aggregation or proteolysis, or interaction with the storage media [60]. The negative impact of the storage conditions can be partially mitigated by designing efficient methods to protect enzymes, including, but not limited to, their immobilisation on solid supports, encapsulation in soft matrices or coating with protective layers such as polymers [53,61]. The stability of the HNS and LAC in solution was assessed after storing the samples for 50 days at 4 °C. The enzymatic activity was assessed based on the oxidation of ABTS, and the residual activity of each sample is presented in Fig. 12, where the initial activity of each sample was considered 100 %.

In the case of the LAC solution stored at 4 °C, approximately 65 % of the catalytic activity was lost after 50 days of storage, demonstrating the instability of the enzyme in solution during long-term storage. On the other hand, in the case of the HNS, better stability can be observed, with about 50 % of the catalytic activity being conserved upon storage. It can be noted that the stability of the HNS increases with the increase in the CHI-*g*-PNIPAM content, suggesting that the grafted polysaccharide has a

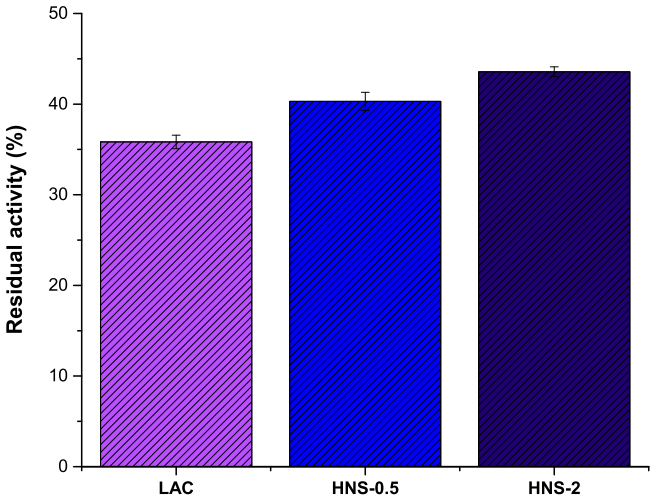

Fig. 12. Residual activity of the free LAC and the LAC/CHI-*g*-PNIPAM HNS after 50 days of storage at 4 °C.

protective effect on the enzyme, preventing its unfolding upon storage. Upon complexation with LAC, CHI-*g*-PNIPAM copolymer can create a protective barrier on the surface of the enzyme, stabilising its structure and reducing its direct exposure to the solvent. The formation of this barrier can potentially minimise the exposure of the enzyme to the solvent or other compounds in the storage media, preserving the structural integrity of the enzyme, as also reported by Prancheva et al., who obtained complexes of $PDMAEMA_{17}$-b-PCL_{70}-b-$PDMAEMA_{17}$ with seratiopeptidase and hyaluronic acid-coated complexes of the same mixture [62].

Additional insights into the preservation or modification of the enzyme conformation upon complexation of LAC with CHI-*g*-PNIPAM can be obtained from the fluorescence spectra of the native enzyme and the corresponding HNS. LAC contains tryptophan (Trp), tyrosine and phenylalanine residues that contribute to its fluorescence properties. Especially Trp residues are valuable in evaluating potential conformational changes in the enzyme structure, since their fluorescence emission is susceptible to changes due to environmental factors or the interaction with oppositely charged compounds. In this context, the fluorescence spectra registered for the initial LAC solution and the corresponding LAC containing HNS can offer important information about potential changes in the conformation of the complexed enzyme. The fluorescence emission spectra were recorded in the range of 300–450 nm upon excitation at 280 nm and are presented in Fig. 13.

The fluorescence spectra obtained for the HNS, in comparison to that of the native LAC, indicate the presence of additional underlying peaks.

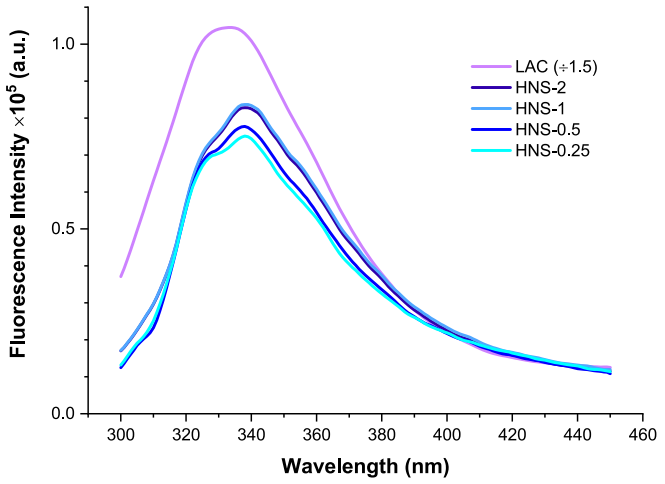

Fig. 13. Fluorescence spectra of the native LAC solution (divided by a factor of 1.5) and of the HNS.

This modification in the emission spectra could be attributed to the contribution of individual Trp residues, which experience different changes in the polarity of their microenvironment [40,63–65]. LAC contains seven Trp residues in total, located at different positions of the enzyme molecule, with some of them being closer to the surface and the rest being located inside the hydrophobic domains of the molecule, as can be observed from the secondary structure of the protein shown in Fig. S6. For this reason, the emission spectra of the HNS, the native LAC, as well as LAC after thermal treatment (at 80 °C for 1 h) for comparison, were deconvoluted into five individual peaks as presented in Fig. S7. The difference in intensity observed for the HNS in comparison to free LAC is the result of the lower concentration of enzyme in the so-formed structures, which was 0.2 mg/mL, compared with the pure enzyme solution that had a concentration of 0.5 mg/mL (note that the spectrum of free LAC in Fig. 13 is divided by a factor of 1.5 for comparison reasons). As far as the position of the peak is concerned, the native LAC emission spectrum presents a maximum at about 332 nm. Upon complexation with the CHI-*g*-PNIPAM, a small red shift (about 5 nm) of the overall emission peak occurs, which suggests some degree of conformational change that could be linked to the exposure of some of the Trp residues to a different environment [66,67]. In particular, from the deconvolution of the spectra, it is evident that the individual peaks that are mostly affected upon complexation with the grafted copolymer are the ones corresponding to higher emissions (i.e., Fit Peaks 4 and 5 of Fig. S7), which apparently correspond to more exposed Trp residues, both showing a redshift of their maximum to a smaller or greater extent, as well as changes of their relative amplitude (see Fig. S8). These observations could most probably mean that the Trp residues of the LAC molecule that are closer to the surface are exposed to a more polar environment after the interaction with the CHI-*g*-PNIPAM copolymer. Another possible explanation is that the occurring electrostatic interactions, as well as hydrogen bonding interactions, between specific Trp and the graft copolymer could stabilise their excited state and lower their energy, thus leading to longer emission wavelengths. Nevertheless, the lower emission wavelength peaks corresponding to the Trp residues located inside hydrophobic domains (i.e., Fit Peaks 1, 2, and 3 of Fig. S7) seem rather unaffected upon complexation. Quite interestingly, the spectrum of thermally treated LAC presents similar changes (Fig. S7b). However, the denaturation of the enzyme is usually evidenced by a parallel significant quenching of its fluorescence intensity [68]. Therefore, we can assume that while there might be some degree of conformational rearrangement of the enzyme's tertiary structure, the enzyme is not completely denatured upon complexation with CHI-*g*-PNIPAM. This assumption is further supported by the observed preservation and even slight enhancement of its enzymatic activity, as previously discussed, which could be a consequence of the partial unfolding of the enzyme molecule, which facilitates the accessibility of the catalytic center.

3.7. Dye degradation

LAC finds important applications in the development of emerging water cleaning technologies due to its capability of degrading various organic pollutants, including dyes, drugs or endocrine disruptors [69,70]. The use of HNS as catalysts for water cleaning applications could be a valuable method, as the embedment of the LAC molecules into complex nanostructures could potentially prevent activity loss and enzyme denaturation during the degradation process. As reported in other studies, LAC can catalyse the degradation of various dyes in the presence of redox mediators such as ABTS or SG [37,71]. In this context, the capacity of the HNS to degrade two model dyes, IC and CR, was studied in the presence of SG as mediator, and the pseudo-first order kinetic model was used to investigate the degradation process (Fig. 14).

The degradation of IC in the presence of free LAC was achieved in about 80 min, while the use of the HNS enhanced the degradation rate, obtaining the complete discolouration of the IC sample in about 45 min in the presence of the HNS-0.5 and 60 min in the presence of the HNS-2. These results emphasise the increased efficiency of the embedded LAC, as also observed during the activity assays. The higher degradation efficiency of the HNS compared with the free LAC can be the result of the interaction between the CHI-*g*-PNIPAM and the IC, which apparently facilitates the interaction between the dye and the enzyme-mediator pair. The increased degradation efficiency of the prepared HNS was also confirmed by the kinetic modelling performed, which evidenced that the degradation rate constants increased 3 times in the case of the HNS compared with the free LAC. Similar observations were reported by Zhang and coauthors, who studied the enzymatic degradation of malachite green and acid orange 7 in the presence of HNS prepared with LAC and poly(ethyleneimine) [44]. The authors evidenced the increased efficiency of the HNS in the degradation of acid orange 7, with a 3-fold increase in the degradation rate as compared to the free LAC. On the other hand, the degradation rate of malachite green was lower, probably due to the structural differences between the two dyes.

The increased efficiency of the HNS in the degradation of IC is additionally supported by comparison with previously reported studies, as presented in Table 3. However, it is important to note that such comparisons are inherently limited by differences in the experimental procedure employed. The degradation process is highly influenced by multiple factors, including the amount of biocatalyst used, the nature and effectiveness of the mediator, the initial dye concentration and the experimental conditions employed. Because these parameters can vary significantly between studies, any comparison should be considered indicative rather than definitive.

As reported in Table 3, LAC-mediated degradation of IC can be successfully employed for bioremediation purposes, various catalytic systems being proposed, including both free and immobilised enzymes. The degradation efficiency obtained is strongly influenced by the accessibility of the catalytic center of the enzyme, a general trend of decreasing efficiency (increasing degradation time) being observed when using biocatalysts with LAC immobilised on solid supports. In this context, the use of HNS, such as the ones proposed in this study, could be a valuable method of mitigating the loss in enzymatic activity resulting from diffusional constraints after immobilisation.

In the case of CR degradation, the efficiency was lower for both free LAC and the HNS, potentially due to the lower affinity between the dye and the enzyme because of the larger and more complex structure of the dye, which makes it more stable to enzymatic degradation [80]. Such a behaviour could also be promoted by electrostatic repulsions between the dye and the polysaccharide coating of the enzyme or by diffusional limitations. This observation is additionally supported by the values of the degradation rate constants, which are lower compared with the

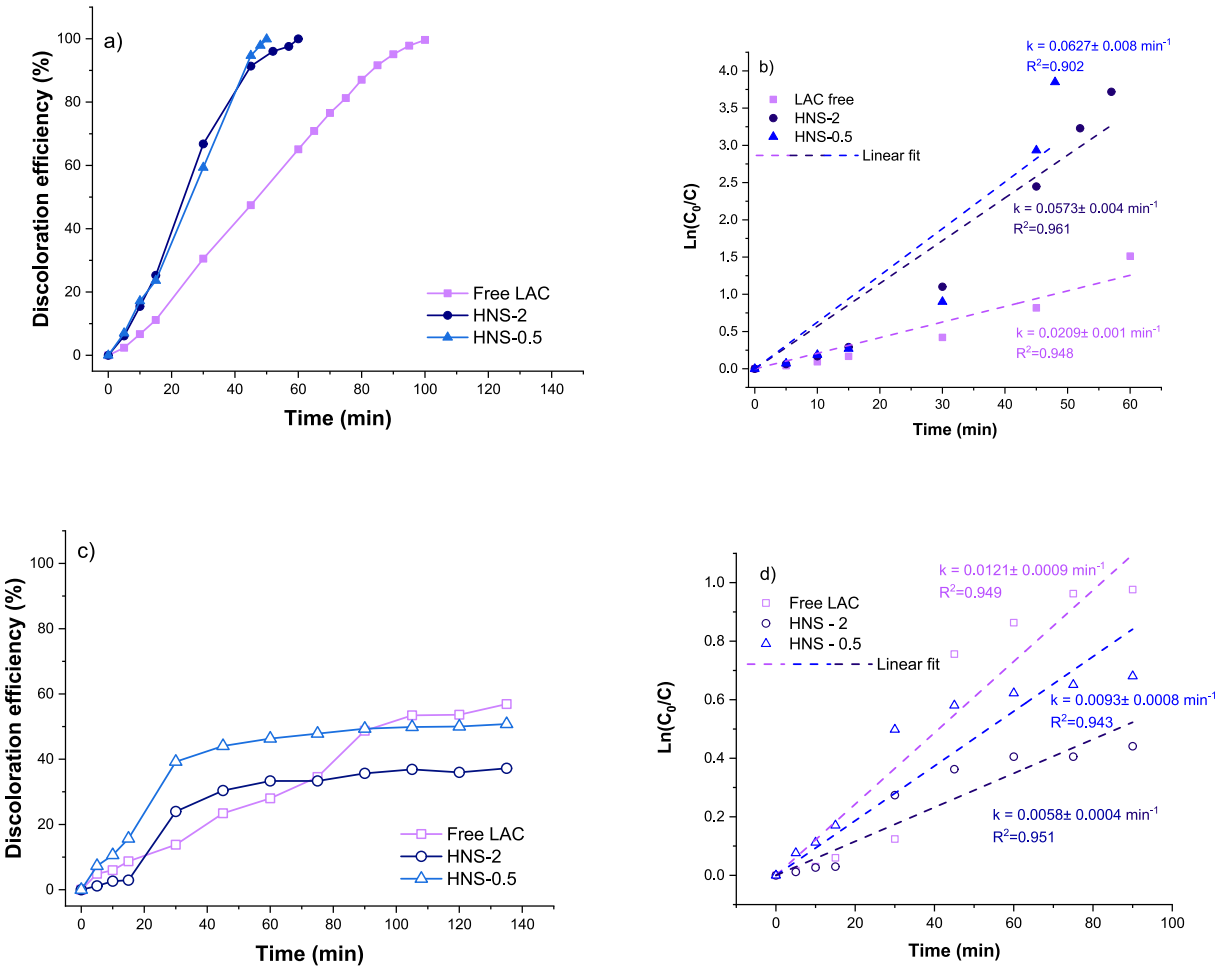

Fig. 14. Discoloration efficiency of IC (a) and CR (c) and pseudo-first order kinetic modelling of IC (b) and CR (d) degradation in the presence of free LAC and of HNS-2 and HNS-0.5, using SG as mediator.

Table 3
Comparison between previously reported studies in the enzymatic degradation of IC.

System:	Reported efficiency:	Reference:
HNS-0.5 with SG as mediator	100 % after 45 min (50 mg/L IC)	This study
HNS-2 with SG as mediator	100 % after 60 min (50 mg/L IC)	This study
LAC spores from HL3 strain and acetosyringone as mediator	100 % after 2 h (47 mg/L IC)	[72]
LAC and ABTS-modified silica as a mediator	95 % after 5 min (20 mg/L IC)	[73]
LAC immobilised on CHI beads	100 % after 8 h (50 mg/L IC)	[74]
LAC immobilised on magnetic zeolitic imidazolate framework−8 nanoparticles and acetosyringone as mediator	100 % after 15 min (25 mg/mL)	[75]
LAC immobilised on CHI beads	56 % after 96 h (50 mg/L IC)	[76]
LAC immobilised on EDTA-Cu (II) chelating magnetic nanoparticles and methyl syringate as mediator	44 % after 4 h (5 mM IC)	[77]
LAC immobilised on lysine functionalized cellulose	99.06 % after 72 h (50 mg/L IC)	[78]
LAC co-immobilised with TiO_2 nanoparticles in alginate beads	~70 % (25 mg/L IC)	[79]

degradation rates obtained for IC. Moreover, the CR degradation rate constant of free LAC was higher compared with the CR degradation rates of the HNS, further confirming the decreased affinity between the dye and the hybrid nanostructures. Nevertheless, the degradation efficiency registered in the case of CR was higher than 50 %, suggesting the potential of both free and complexed LAC to degrade CR.

4. Conclusions

This study investigated the formation of HNS based on electrostatic interactions between the LAC from *Trametes versicolor* and a CHI-*g*-PNIPAM copolymer. The characterization methodology employed in this study, consisting of a combination of DLS, ELS, STEM, MD simulations and fluorescence spectroscopy, demonstrated the successful formation of the HNS, emphasising the role of the grafted polysaccharide in the overall properties and the behaviour of the formed nanostructures. In particular, the content of CHI-*g*-PNIPAM influences the size, charge, structure and morphology of the formed HNS. Moreover, the LAC/CHI-*g*-PNIPAM complexes preserved the thermoresponsive behaviour characteristic of the copolymer due to the presence of the PNIPAM side chains and exhibited satisfactory stability to ionic strength. Furthermore, the study examined the preservation of the enzymatic activity upon binding of LAC with CHI-*g*-PNIPAM, observing an enhancement of 3 % to 17 % of the catalytic activity compared with the free LAC and a prolonged stability of the HNS at pH and temperature variations, together with an extended storage stability. Yet, the proposed systems present limitations in terms of reusability, as their separation from the reaction media needs

further study. Additionally, the HNS with embedded LAC were tested in the degradation of dyes in aqueous solutions. With 100 % efficiency in the degradation of IC and roughly 50 % efficiency in CR degradation, the HNS show enhanced capacity to act as catalysts for water cleaning applications.

CRediT authorship contribution statement

Larisa-Maria Petrila: Visualization, Validation, Methodology, Investigation, Formal analysis, Data curation, Conceptualization, Writing – review & editing, Writing – original draft. **Maria Karayianni:** Methodology, Investigation, Formal analysis, Data curation, Conceptualization, Writing – review & editing, Writing – original draft. **Tudor Vasiliu:** Methodology, Investigation, Data curation, Conceptualization. **Răzvan Puf:** Methodology, Investigation, Data curation, Conceptualization. **Marcela Mihai:** Validation, Supervision, Project administration, Funding acquisition, Writing – review & editing, Writing – original draft. **Stergios Pispas:** Validation, Supervision, Project administration, Funding acquisition, Writing – review & editing.

Funding

This work was financially supported by the Romanian Authority for Research, with project number PNRR-III-C9-2022-I8-201, within the National Recovery and Resilience Plan and by European Union's Horizon Europe research and innovation programme under grant agreement No 101086667, project BioMat4CAST (BioMat4CAST - Petru Poni Institute of Macromolecular Chemistry Multi-Scale In Silico Laboratory for Complex and Smart Biomaterials).

Declaration of competing interest

The authors declare that they have no known competing financial interests or personal relationships that could have appeared to influence the work reported in this paper.

Acknowledgements

Dr. Daniela Rusu and Dr. Radu Ionuț Tigoianu from Petru Poni Institute of Macromolecular Chemistry are kindly acknowledged for performing the STEM and the fluorescence spectroscopy measurements, respectively.

Appendix A. Supplementary data

Supplementary data to this article can be found online at https://doi.org/10.1016/j.ijbiomac.2025.146754.

Data availability

Data will be made available on request.

References

[1] J.K. Bediako, Y. El Ouardi, E.S. Massima Mouele, B. Mensah, E. Repo, Polyelectrolyte and polyelectrolyte complex-incorporated adsorbents in water and wastewater remediation – a review of recent advances, Chemosphere 325 (2023) 138418, https://doi.org/10.1016/J.CHEMOSPHERE.2023.138418.
[2] S. Mehta, A. Suresh, Y. Nayak, R. Narayan, U.Y. Nayak, Hybrid nanostructures: versatile systems for biomedical applications, Coord. Chem. Rev. 460 (2022) 214482, https://doi.org/10.1016/J.CCR.2022.214482.
[3] J. van der Gucht, E. Spruijt, M. Lemmers, M.A. Cohen Stuart, Polyelectrolyte complexes: bulk phases and colloidal systems, J. Colloid Interface Sci. 361 (2011) 407–422, https://doi.org/10.1016/j.jcis.2011.05.080.
[4] S. Morariu, M. Avadanei, L.E. Nita, Effect of pH on the poly(acrylic acid)/poly (vinyl alcohol)/lysozyme complexes formation, Molecules 29 (2024) 208, https://doi.org/10.3390/MOLECULES29010208.
[5] A. Varadarajan, L.T. Kearney, J.K. Keum, A.K. Naskar, S. Kundu, Effects of salt on phase behavior and rheological properties of alginate–chitosan polyelectrolyte complexes, Biomacromolecules 24 (2023) 2730–2740, https://doi.org/10.1021/ACS.BIOMAC.3C00171.
[6] E.S. Dragan, M. Mihai, S. Schwarz, Polyelectrolyte complex dispersions with a high colloidal stability controlled by the polyion structure and titrant addition rate, Colloids Surf. A Physicochem. Eng. Asp. 290 (2006) 213–221, https://doi.org/10.1016/J.COLSURFA.2006.05.022.
[7] I.A. Dinu, M. Mihai, E.S. Dragan, Comparative study on the formation and flocculation properties of polyelectrolyte complex dispersions based on synthetic and natural polycations, Chem. Eng. J. 160 (2010) 115–121, https://doi.org/10.1016/J.CEJ.2010.03.018.
[8] A. Reisch, P. Tirado, E. Roger, F. Boulmedais, D. Collin, J.C. Voegel, B. Frisch, P. Schaaf, J.B. Schlenoff, Compact saloplastic poly(acrylic acid)/poly(allylamine) complexes: kinetic control over composition, microstructure, and mechanical properties, Adv. Funct. Mater. 23 (2013) 673–682, https://doi.org/10.1002/adfm.201201413.
[9] M. Mihai, E.S. Dragan, S. Schwarz, A. Janke, Dependency of particle sizes and colloidal stability of polyelectrolyte complex dispersions on polyanion structure and preparation mode investigated by dynamic light scattering and atomic force microscopy, J. Phys. Chem. B 111 (2007) 8668–8675, https://doi.org/10.1021/JP071655Q.
[10] T. Delair, Colloidal polyelectrolyte complexes of chitosan and dextran sulfate towards versatile nanocarriers of bioactive molecules, Eur. J. Pharm. Biopharm. 78 (2011) 10–18, https://doi.org/10.1016/j.ejpb.2010.12.001.
[11] S.L. Turgeon, C. Schmitt, C. Sanchez, Protein-polysaccharide complexes and coacervates, Curr. Opin. Colloid Interface Sci. 12 (2007) 166–178, https://doi.org/10.1016/j.cocis.2007.07.007.
[12] Y.A. Antonov, I.L. Zhuravleva, R. Cardinaels, P. Moldenaers, Macromolecular complexes of lysozyme with kappa carrageenan, Food Hydrocoll. 74 (2018) 227–238, https://doi.org/10.1016/j.foodhyd.2017.07.022.
[13] C.J.F. Souza, E.E. Garcia-Rojas, C.S.F. Souza, L.C. Vriesmann, J. Vicente, M.G. de Carvalho, C.L.O. Petkowicz, C.S. Favaro-Trindade, Immobilization of β-galactosidase by complexation: effect of interaction on the properties of the enzyme, Int. J. Biol. Macromol. 122 (2019) 594–602, https://doi.org/10.1016/j.ijbiomac.2018.11.007.
[14] R.C.F. Cheung, T.B. Ng, J.H. Wong, W.Y. Chan, Chitosan: an update on potential biomedical and pharmaceutical applications, Mar. Drugs 13 (2015) 5156–5186, https://doi.org/10.3390/MD13085156.
[15] A. Barakat, G.A.M. Ehagali, E.A. Kamoun, M.S. Abusaif, M.E. Owda, M.B. Ghazy, Y. A. Ammar, A novel chitosan-Schiff bases bearing a new quinoxaline moiety as an approach for potent antimicrobial agent: synthesis, characterization and in vitro assessments, Carbohydr. Polym. 352 (2025) 123205, https://doi.org/10.1016/J.CARBPOL.2024.123205.
[16] T.U. Wani, A.H. Pandith, F.A. Sheikh, Polyelectrolytic nature of chitosan: influence on physicochemical properties and synthesis of nanoparticles, J. Drug Deliv. Sci. Technol. 65 (2021) 102730, https://doi.org/10.1016/J.JDDST.2021.102730.
[17] M. Ul-Islam, K.F. Alabbosh, S. Manan, S. Khan, F. Ahmad, M.W. Ullah, Chitosan-based nanostructured biomaterials: synthesis, properties, and biomedical applications, Adv. Ind. Eng. Polym. Res. 7 (2024) 79–99, https://doi.org/10.1016/J.AIEPR.2023.07.002.
[18] M. Pakizeh, A. Moradi, T. Ghassemi, Chemical extraction and modification of chitin and chitosan from shrimp shells, Eur. Polym. J. 159 (2021) 110709, https://doi.org/10.1016/J.EURPOLYMJ.2021.110709.
[19] E.M. Elnaggar, M.S. Abusaif, Y.M. Abdel-Baky, A. Ragab, A.M. Omer, I. Ibrahim, Y. A. Ammar, Insight into divergent chemical modifications of chitosan biopolymer: review, Int. J. Biol. Macromol. 277 (2024) 134347, https://doi.org/10.1016/J.IJBIOMAC.2024.134347.
[20] T.J. Madera-Santana, C.H. Herrera-Méndez, J.R. Rodríguez-Núñez, An overview of the chemical modifications of chitosan and their advantages, Green Mater. 6 (2018) 131–142, https://doi.org/10.1680/JGRMA.18.00053.
[21] H.S. Tsai, Y.Z. Wang, J.J. Lin, W.F. Lien, Preparation and properties of sulfopropyl chitosan derivatives with various sulfonation degree, J. Appl. Polym. Sci. 116 (2010) 1686–1693, https://doi.org/10.1002/APP.31689.
[22] M.M. Zaharia, F. Bucatariu, M. Karayianni, E.D. Lotos, M. Mihai, S. Pispas, Synthesis of thermoresponsive chitosan-graft-poly(N-isopropylacrylamide) hybrid copolymer and its complexation with DNA, Polymers 16 (2024) 1315, https://doi.org/10.3390/polym16101315.
[23] D. Selianitis, S. Pispas, PDEGMA-b-PDIPAEMA copolymers via RAFT polymerization and their pH and thermoresponsive schizophrenic self-assembly in aqueous media, J. Polym. Sci. 58 (2020) 1867–1880, https://doi.org/10.1002/POL.20200266.
[24] M.J. Ansari, R.R. Rajendran, S. Mohanto, U. Agarwal, K. Panda, K. Dhotre, R. Manne, A. Deepak, A. Zafar, M. Yasir, S. Pramanik, Poly(N-isopropylacrylamide)-based hydrogels for biomedical applications: a review of the state-of-the-art, Gels 8 (2022) 454, https://doi.org/10.3390/GELS8070454.
[25] V.Y. Grinberg, T.V. Burova, N.V. Grinberg, A.P. Moskalets, A.S. Dubovik, I. G. Plashchina, A.R. Khokhlov, Energetics and mechanisms of poly(N-isopropylacrylamide) phase transitions in water-methanol solutions, Macromolecules 53 (2020) 10765–10772, https://doi.org/10.1021/ACS.MACROMOL.0C02253.
[26] K. Yanase, R. Buchner, T. Sato, Microscopic insights into the phase transition of poly(N-isopropylacrylamide) in aqueous media: effects of molecular weight and polymer concentration, J. Mol. Liq. 302 (2020) 112025, https://doi.org/10.1016/J.MOLLIQ.2019.112025.
[27] J. An, G. Li, Y. Zhang, T. Zhang, X. Liu, F. Gao, M. Peng, Y. He, H. Fan, Recent advances in enzyme-nanostructure biocatalysts with enhanced activity, Catalysts 10 (2020) 338, https://doi.org/10.3390/catal10030338.

[28] J. Chapman, A.E. Ismail, C.Z. Dinu, Industrial applications of enzymes: recent advances, techniques, and outlooks, Catalysts 8 (2018) 238, https://doi.org/10.3390/catal8060238.
[29] C. Waltmann, C.E. Mills, J. Wang, B. Qiao, J.M. Torkelson, D. Tullman-Ercek, M. O. de la Cruz, Functional enzyme–polymer complexes, Proc. Natl. Acad. Sci. U. S. A. 119 (2022) e2119509119, https://doi.org/10.1073/PNAS.2119509119.
[30] Y.A. Antonov, I.L. Zhuravleva, R. Cardinaels, P. Moldenaers, Structural studies on the interaction of lysozyme with dextran sulfate, Food Hydrocoll. 44 (2015) 71–80, https://doi.org/10.1016/j.foodhyd.2014.09.006.
[31] D. Fotaki, M. Karayianni, A. Skandalis, E. Haladjova, A. Forys, B. Trzebicka, S. Rangelov, S. Pispas, Complexation of poly(methacrylic acid) star polyelectrolytes with lysozyme, Eur. Polym. J. 206 (2024) 112773, https://doi.org/10.1016/J.EURPOLYMJ.2024.112773.
[32] W. Jin, Z. Wang, D. Peng, W. Shen, Z. Zhu, S. Cheng, B. Li, Q. Huang, Effect of linear charge density of polysaccharides on interactions with α-amylase: self-assembling behavior and application in enzyme immobilization, Food Chem. 331 (2020) 127320, https://doi.org/10.1016/j.foodchem.2020.127320.
[33] S. Kübelbeck, J. Mikhael, S. Schoof, A. Andrieu-Brunsen, G. Baier, Immobilization of α-amylase in polyelectrolyte complexes, J. Appl. Polym. Sci. 134 (2017) 45036, https://doi.org/10.1002/app.45036.
[34] A.V. Briones, T. Sato, Encapsulation of glucose oxidase (GOD) in polyelectrolyte complexes of chitosan-carrageenan, React. Funct. Polym. 70 (2010) 19–27, https://doi.org/10.1016/j.reactfunctpolym.2009.09.009.
[35] Y. Du, L. Zhao, Z. Geng, Z. Huo, H. Li, X. Shen, X. Peng, R. Yan, J. Cui, S. Jia, Construction of catalase@hollow silica nanosphere: catalase with immobilized but not rigid state for improving catalytic performances, Int. J. Biol. Macromol. 263 (2024) 130381, https://doi.org/10.1016/J.IJBIOMAC.2024.130381.
[36] J. Zdarta, S.B. Sigurdardóttir, K. Jankowska, M. Pinelo, Laccase immobilization in polyelectrolyte multilayer membranes for 17α-ethynylestradiol removal: biocatalytic approach for pharmaceuticals degradation, Chemosphere 304 (2022) 135374, https://doi.org/10.1016/j.chemosphere.2022.135374.
[37] L.M. Petrila, F. Bucatariu, I. Stoica, M. Mihai, R. Froidevaux, A green approach combining polyelectrolyte-based core-shell microparticles and laccase for indigo carmine degradation, J. Environ. Chem. Eng. 13 (2025) 115631, https://doi.org/10.1016/J.JECE.2025.115631.
[38] M. Maryšková, M. Schaabová, H. Tománková, V. Novotnỳ, M. Rysová, Wastewater treatment by novel polyamide/polyethylenimine nanofibers with immobilized laccase, Water 12 (588) (2020), https://doi.org/10.3390/w12020588.
[39] J. Hixon, Y.K. Reshetnyak, Algorithm for the analysis of tryptophan fluorescence spectra and their correlation with protein structural parameters, Algorithms 2 (2009) 1155–1176, https://doi.org/10.3390/A2031155.
[40] K. Piontek, M. Antorini, T. Choinowski, Crystal structure of a laccase from the fungus Trametes versicolor at 1.90-A resolution containing a full complement of coppers, J. Biol. Chem. 277 (2002) 37663–37669, https://doi.org/10.1074/JBC.M204571200.
[41] T. Bertrand, C. Jolivalt, P. Briozzo, E. Caminade, N. Joly, C. Madzak, C. Mougin, Crystal structure of a four-copper laccase complexed with an arylamine: insights into substrate recognition and correlation with kinetics, Biochemistry 41 (2002) 7325–7333, https://doi.org/10.1021/BI0201318.
[42] D.A. Case, H.M. Aktulga, K. Belfon, D.S. Cerutti, G.A. Cisneros, V.W.D. Cruzeiro, N. Forouzesh, T.J. Giese, A.W. Götz, H. Gohlke, S. Izadi, K. Kasavajhala, M. C. Kaymak, E. King, T. Kurtzman, T.S. Lee, P. Li, J. Liu, T. Luchko, R. Luo, M. Manathunga, M.R. Machado, H.M. Nguyen, K.A. O'Hearn, A.V. Onufriev, F. Pan, S. Pantano, R. Qi, A. Rahnamoun, A. Risheh, S. Schott-Verdugo, A. Shajan, J. Swails, J. Wang, H. Wei, X. Wu, Y. Wu, S. Zhang, S. Zhao, Q. Zhu, T.E. Cheatham, D.R. Roe, A. Roitberg, C. Simmerling, D.M. York, M.C. Nagan, K.M. Merz, AmberTools, J. Chem. Inf. Model. 63 (2023) 6183–6191, https://doi.org/10.1021/ACS.JCIM.3C01153.
[43] M.J. Abraham, T. Murtola, R. Schulz, S. Páll, J.C. Smith, B. Hess, E. Lindah, GROMACS: high performance molecular simulations through multi-level parallelism from laptops to supercomputers, SoftwareX 1-2 (2015) 19–25, https://doi.org/10.1016/J.SOFTX.2015.06.001.
[44] X. Zhang, M. Hua, L. Lv, B. Pan, Ionic polymer-coated laccase with high activity and enhanced stability: application in the decolourisation of water containing AO7, Sci. Rep. 5 (2015) 1–9, https://doi.org/10.1038/srep08253.
[45] A. Kołodziejczak-Radzimska, J. Zembrzuska, K. Siwińska-Ciesielczyk, T. Jesionowski, Catalytic and physicochemical evaluation of a TiO2/ZnO/laccase biocatalytic system: application in the decolorization of azo and anthraquinone dyes, Materials 14 (2021) 6030, https://doi.org/10.3390/MA14206030.
[46] X. Wang, K. Zheng, Y. Si, X. Guo, Y. Xu, Protein–polyelectrolyte interaction: thermodynamic analysis based on the titration method, Polymers 11 (2019) 82, https://doi.org/10.3390/POLYM11010082.
[47] F.L.B. Da Silva, B. Jönsson, Polyelectrolyte–protein complexation driven by charge regulation, Soft Matter 5 (2009) 2862–2868, https://doi.org/10.1039/B902039J.
[48] Q. Huajun, X. Caixia, H. Xirong, D. Yi, Q. Yinbo, G. Peiji, Immobilization of laccase on nanoporous gold: comparative studies on the immobilization strategies and the particle size effects, J. Phys. Chem. C 113 (2009) 2521–2525, https://doi.org/10.1021/JP8090304.
[49] S. Shleev, C.T. Reimann, V. Serezhenkov, D. Burbaev, A.I. Yaropolov, L. Gorton, T. Ruzgas, Autoreduction and aggregation of fungal laccase in solution phase: possible correlation with a resting form of laccase, Biochimie 88 (2006) 1275–1285, https://doi.org/10.1016/J.BIOCHI.2006.02.007.
[50] B. Panganiban, B. Qiao, T. Jiang, C. Delre, M.M. Obadia, T.D. Nguyen, A.A. A. Smith, A. Hall, I. Sit, M.G. Crosby, P.B. Dennis, E. Drockenmuller, M.O. De La Cruz, T. Xu, Random heteropolymers preserve protein function in foreign environments, Science 359 (2018) 1239–1243, https://doi.org/10.1126/science.aao0335.
[51] L. Gärdlund, L. Wågberg, M. Norgren, New insights into the structure of polyelectrolyte complexes, J. Colloid Interface Sci. 312 (2007) 237–246, https://doi.org/10.1016/j.jcis.2007.03.075.
[52] V.S. Meka, M.K.G. Sing, M.R. Pichika, S.R. Nali, V.R.M. Kolapalli, P. Kesharwani, A comprehensive review on polyelectrolyte complexes, Drug Discov. Today 22 (2017) 1697–1706, https://doi.org/10.1016/j.drudis.2017.06.008.
[53] L.M. Petrila, V.R. Grădinaru, F. Bucatariu, M. Mihai, Polymer/enzyme composite materials—versatile catalysts with multiple applications, Chemistry 4 (2022) 1312–1338, https://doi.org/10.3390/CHEMISTRY4040087.
[54] B. Çalbaş, A.N. Keobounnam, C. Korban, A.J. Doratan, T. Jean, A.Y. Sharma, T. A. Wright, Protein–polymer bioconjugation, immobilization, and encapsulation: a comparative review towards applicability, functionality, activity, and stability, Biomater. Sci. 12 (2024) 2841–2864, https://doi.org/10.1039/D3BM01861J.
[55] V.I. Muronetz, D.V. Pozdyshev, P.I. Semenyuk, Polyelectrolytes for enzyme immobilization and the regulation of their properties, Polymers 14 (19) (2022) 4204, https://doi.org/10.3390/polym14194204.
[56] Y. Wan, Y. Qiu, J. Zhou, J. Liu, M.A.C. Stuart, Y. Peng, J. Wang, Stable and permeable polyion complex vesicles designed as enzymatic nanoreactors, Soft Matter 20 (2024) 3499–3507, https://doi.org/10.1039/D4SM00216D.
[57] Z. Wang, D. Ren, Y. Cheng, X. Zhang, S. Zhang, W. Chen, Immobilization of laccase on chitosan functionalized halloysite nanotubes for degradation of bisphenol A in aqueous solution: degradation mechanism and mineralization pathway, Heliyon 8 (2022) e09919, https://doi.org/10.1016/J.HELIYON.2022.E09919.
[58] I.A. Veselova, A.V. Kireiko, T.N. Shekhovtsova, Catalytic activity and the stability of horseradish peroxidase increase as a result of its incorporation into a polyelectrolyte complex with chitosan, Appl. Biochem. Microbiol. 45 (2009) 125–129, https://doi.org/10.1134/S0003683809020021.
[59] H. Jia, C. Zhong, F. Huang, C. Wang, L. Jia, H. Zhou, P. Wei, The preparation and characterization of a laccase nanogel and its application in naphthoquinone synthesis, Chempluschem 78 (2013) 451–458, https://doi.org/10.1002/CPLU.201300066.
[60] R.A. Sheldon, S. van Pelt, Enzyme immobilisation in biocatalysis: why, what and how, Chem. Soc. Rev. 42 (2013) 6223–6235, https://doi.org/10.1039/c3cs60075k.
[61] J. Zdarta, A.S. Meyer, T. Jesionowski, M. Pinelo, A general overview of support materials for enzyme immobilization: characteristics, properties, practical utility, Catalysts 8 (2018) 92, https://doi.org/10.3390/catal8020092.
[62] A. Prancheva, K. Kamenova, P.D. Petrov, Hyaluronic acid-coated complexes of cationic polymeric micelles and serratiopeptidase—preparation, characterization, and enzyme activity, J. Polym. Sci. 0 (2025) 1–13, https://doi.org/10.1002/POL.20250185.
[63] J.L. Meagher, J.M. Beechem, S.T. Olson, P.G.W. Gettinst, Deconvolution of the fluorescence emission spectrum of human antithrombin and identification of the tryptophan residues that are responsive to heparin binding, J. Biol. Chem. 273 (1998) 23283–23289, https://doi.org/10.1074/jbc.273.36.23283.
[64] J.-M. Glandières, C. Twist, A. Haouz, C. Zentz, B. Alpert, Resolved fluorescence of the two tryptophan residues in horse apomyoglobin, Photochem. Photobiol. 71 (2007) 382–386, https://doi.org/10.1562/0031-8655(2000)0710382rfottt2.0.co2.
[65] A. Sundaramoorthy, G. Bharanidharan, A. Prakasarao, S. Ganesan, Characterization and classification of pathogenic bacteria using native fluorescence and spectral deconvolution, J. Biophotonics 17 (2024) e202300566, https://doi.org/10.1002/jbio.202300566.
[66] Y. Zhang, D. Rochefort, Activity, conformation and thermal stability of laccase and glucose oxidase in poly(ethyleneimine) microcapsules for immobilization in paper, Process Biochem. 46 (2011) 993–1000, https://doi.org/10.1016/J.PROCBIO.2011.01.006.
[67] F.H. dos Santos Rodrigues, G.G. Delgado, T. Santana da Costa, L. Tasic, Applications of fluorescence spectroscopy in protein conformational changes and intermolecular contacts, BBA Advances 3 (2023) 100091, https://doi.org/10.1016/J.BBADVA.2023.100091.
[68] O. Saoudi, N. Ghaouar, T. Othman, Fluorescence study of laccase from Trametes versicolor under the effects of pH, chemical denaturants and ionic liquids, J. Mol. Liq. 225 (2017) 56–63, https://doi.org/10.1016/J.MOLLIQ.2016.11.050.
[69] Q. Lou, Y. Wu, H. Ding, B. Zhang, W. Zhang, Y. Zhang, L. Han, M. Liu, T. He, J. Zhong, Degradation of sulfonamides in aquaculture wastewater by laccase–syringaldehyde mediator system: response surface optimization, degradation kinetics, and degradation pathway, J. Hazard. Mater. 432 (2022) 128647, https://doi.org/10.1016/J.JHAZMAT.2022.128647.
[70] W. Zhou, W. Zhang, Y. Cai, Laccase immobilization for water purification: a comprehensive review, Chem. Eng. J. 403 (2021) 126272, https://doi.org/10.1016/j.cej.2020.126272.
[71] A. Yadav, P. Yadav, A. Kumar Singh, V. kumar, V. Chintaman Sonawane, Markandeya, R. Naresh Bharagava, A. Raj, Decolourisation of textile dye by laccase: process evaluation and assessment of its degradation bioproducts, Bioresour. Technol. 340 (2021) 125591, https://doi.org/10.1016/J.BIORTECH.2021.125591.
[72] C. Wang, S. Wang, J. Zhang, S. Jiang, D. Cui, H. Sun, C. Liu, L. Li, M. Zhao, The biodegradation of indigo carmine by *bacillus safensis* HL3 spore and toxicity analysis of the degradation products, Molecules 27 (2022) 8539, https://doi.org/10.3390/MOLECULES27238539/S1.
[73] Y. Liu, M. Yan, Y. Geng, J. Huang, ABTS-modified silica nanoparticles as laccase mediators for decolorization of indigo carmine dye, J. Chem. 2015 (2015) 670194, https://doi.org/10.1155/2015/670194.

[74] N. Jaiswal, V.P. Pandey, U.N. Dwivedi, Immobilization of papaya laccase in chitosan led to improved multipronged stability and dye discoloration, Int. J. Biol. Macromol. 86 (2016) 288–295, https://doi.org/10.1016/J.IJBIOMAC.2016.01.079.

[75] J. Wang, S. Yu, F. Feng, L. Lu, Simultaneous purification and immobilization of laccase on magnetic zeolitic imidazolate frameworks: recyclable biocatalysts with enhanced stability for dye decolorization, Biochem. Eng. J. 150 (2019) 107285, https://doi.org/10.1016/J.BEJ.2019.107285.

[76] H.F. Ma, G. Meng, B.K. Cui, J. Si, Y.C. Dai, Chitosan crosslinked with genipin as supporting matrix for biodegradation of synthetic dyes: laccase immobilization and characterization, Chem. Eng. Res. Des. 132 (2018) 664–676, https://doi.org/10.1016/J.CHERD.2018.02.008.

[77] R.A. Fernandes, A.L. Daniel-da-Silva, A.P.M. Tavares, A.M.R.B. Xavier, EDTA-Cu (II) chelating magnetic nanoparticles as a support for laccase immobilization, Chem. Eng. Sci. 158 (2017) 599–605, https://doi.org/10.1016/J.CES.2016.11.011.

[78] N.B. Haro-Mares, J.C. Meza-Contreras, F.A. López-Dellamary, A. Richaud, F. Méndez, B.G. Curiel-Olague, G. Buntkowsky, R. Manríquez-González, Lysine functionalized cellulose for a zwitterion-based immobilization of laccase enzyme and removal of commercial dyes from aqueous media, Surf. Interfaces 35 (2022) 102412, https://doi.org/10.1016/J.SURFIN.2022.102412.

[79] M. Khakshoor, A. Makhdoumi, A. Asoodeh, M.R. Hosseindokht, Co-immobilized spore laccase/TiO_2 nanoparticles in the alginate beads enhance dye removal by two-step decolorization, Environ. Sci. Pollut. Res. 28 (2021) 6099–6110, https://doi.org/10.1007/S11356-020-10901-1.

[80] I. Stoilova, A. Krastanov, V. Stanchev, I. Stoilova, A. Krastanov, V. Stanchev, Properties of crude laccase from Trametes versicolor produced by solid-substrate fermentation, Adv. Biosci. Biotechnol. 1 (2010) 208–215, https://doi.org/10.4236/ABB.2010.13029.